iScience

CellPress
OPEN ACCESS

Article

SnRNA-seq reveals the heterogeneity of spinal ventral horn and mechanism of motor neuron axon regeneration

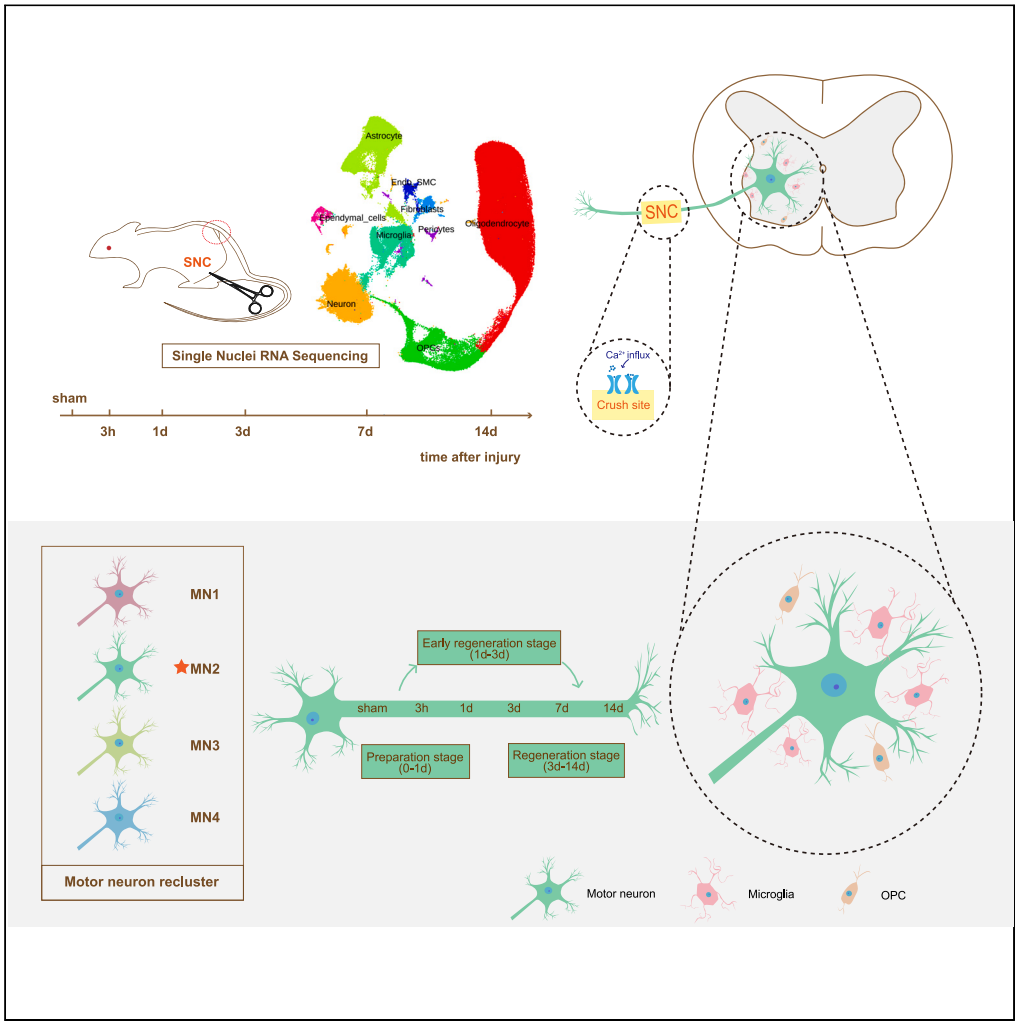

Ye Zhu, Chengcheng Luan, Leilei Gong, ..., Qi Shan, Xiaosong Gu, Songlin Zhou

nervegu@ntu.edu.cn (X.G.)
songlin.zhou@ntu.edu.cn (S.Z.)

Highlights

Our work proposed three stages of spinal motor neuron axon regeneration after SNC

SnRNA-seq revealed the heterogeneity of spinal ventral horn cells after SNC

Regeneration occurred in MN2, aided by Mg6 and the potential supplement of OPC

The key role of Cacna2d2 in motor neurons after SNC had been discovered and verified

Zhu et al., iScience 26, 107264
August 18, 2023
https://doi.org/10.1016/j.isci.2023.107264

iScience

CellPress
OPEN ACCESS

Article

SnRNA-seq reveals the heterogeneity of spinal ventral horn and mechanism of motor neuron axon regeneration

Ye Zhu,[1] Chengcheng Luan,[1] Leilei Gong,[2] Yun Gu,[2] Xinghui Wang,[2] Hualin Sun,[2] Zhifeng Chen,[2] Qiang Zhou,[2] Chang Liu,[2] Qi Shan,[1] Xiaosong Gu,[1,2,*] and Songlin Zhou[2,3,*]

SUMMARY

Spinal motor neurons, the distinctive neurons of the central nervous system, extend into the peripheral nervous system and have outstanding ability of axon regeneration after injury. Here, we explored the heterogeneity of spinal ventral horn cells after rat sciatic nerve crush via single-nuclei RNA sequencing. Interestingly, regeneration mainly occurred in a Sncg$^+$ and Anxa2$^+$ motor neuron subtype (MN2) surrounded by a newly emerged microglia subtype (Mg6) after injury. Subsequently, microglia depletion slowed down the regeneration of sciatic nerve. OPCs were also involved into the regeneration process. Knockdown of Cacna2d2 *in vitro* and systemic blocking of Cacna2d2 *in vivo* improved the axon growth ability, hinting us the importance of Ca^{2+}. Ultimately, we proposed three possible phases of motor neuron axon regeneration: preparation stage, early regeneration stage, and regeneration stage. Taken together, our study provided a resource for deciphering the underlying mechanism of motor neuron axon regeneration in a single cell dimension.

INTRODUCTION

Along with the developmental process, the extension ability of neuron axons will gradually recede, so after axon injury in adult animals, the regeneration ability of neurons is typically weak, especially the central neuron axons. The distal portion of the axon disconnects from the cell body and undergoes Wallerian degeneration, reverse axoplasmic conduction is blocked, and associated neurons in the spinal cord degenerate to vary degrees after peripheral nerve injury (PNI).[1] If the injury is serious, irreversible events such as death or apoptosis will occur. On the contrary, when the situation is not serious, only ultrastructural changes will occur.[2] Ideally, driven by intrinsic regenerative capacity of neurons, surviving neurons can grow a nascent axis and then reconnect and innervate their target organs, thereby restoring function.[3,4]

Compared with the peripheral nervous system (PNS), the regeneration of the central nervous system (CNS) is more difficult. Even if the axons belong to the dorsal root ganglia (DRG), the regeneration of the central branch axons is much more difficult than the peripheral branches connecting the peripheral muscles.[5,6] This is because of the lack of intrinsic regenerative capacity in the CNS and the presence of more inhibitory molecules of regeneration than in the PNS, such as myelin-associated glycoprotein (MAG) and chondroitin sulfate proteoglycans (CSPGs).[7]

Regeneration after injury involves a series of cellular and molecular events, including calcium influx, mitochondrial energy transport, cytoskeleton reorganization, growth cone formation, etc., among which many molecules are involved. The nuclear export of histone deacetylase 5 (HDAC5) caused by axonal injury activates histone acetylation and has a positive effect on regeneration. Calcium influx after axonal injury is deemed to be an essential event supporting axonal regeneration in various organisms.[8,9] Calcium influx leads to elevated cAMP levels that promote axonal fusion in *C. elegans* sensory neurons via downstream dual leucine zipper kinase (DLK-1) signaling.[8,10] Overexpression of doublecortin-like kinase (DCLK) can also promote growth cone formation by maintaining microtubule homeostasis.[11] Deletion of phosphatase and tensin homolog (PTEN) antagonizes the action of PI3K and inactivates mTOR signaling, thereby promoting axonal regeneration in adult retinal ganglion cells (RGCs) and adult sensory neurons.[12,13] Deletion of suppressor of cytokine signaling 3 (SOCS3) alone promotes optic nerve axon growth by inhibiting the

[1]Academy of Medical Engineering and Translational Medicine, Tianjin University, Tianjin 300000, China

[2]Key Laboratory of Neuroregeneration of Jiangsu and Ministry of Education, Co-innovation Center of Neuroregeneration, NMPA Key Laboratory for Research and Evaluation of Tissue Engineering Technology Products, Nantong University, Nantong, Jiangsu 226001, China

[3]Lead contact

*Correspondence: nervegu@ntu.edu.cn (X.G.), songlin.zhou@ntu.edu.cn (S.Z.)

https://doi.org/10.1016/j.isci.2023.107264

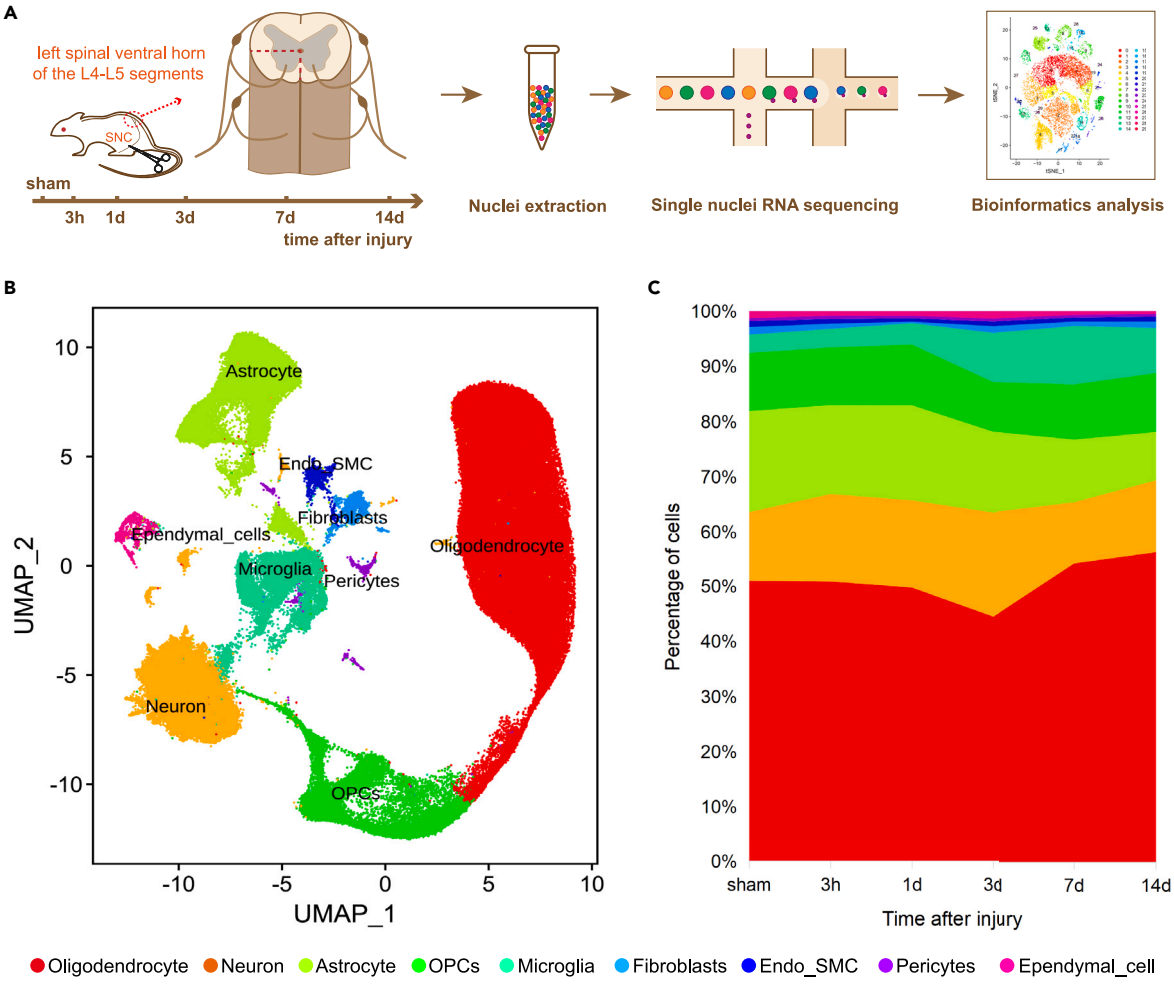
A
left spinal ventral horn
of the L4-L5 segments
SNC
sham
3h
1d
3d
7d
14d
time after injury
Nuclei extraction
Single nuclei RNA sequencing
Bioinformatics analysis
B
Astrocyte
Endo_SMC
Fibroblasts
Ependymal_cells
Microglia
Pericytes
Oligodendrocyte
Neuron
OPCs
UMAP_2
UMAP_1
C
Percentage of cells
Time after injury
sham
3h
1d
3d
7d
14d
Oligodendrocyte
Neuron
Astrocyte
OPCs
Microglia
Fibroblasts
Endo_SMC
Pericytes
Ependymal_cell

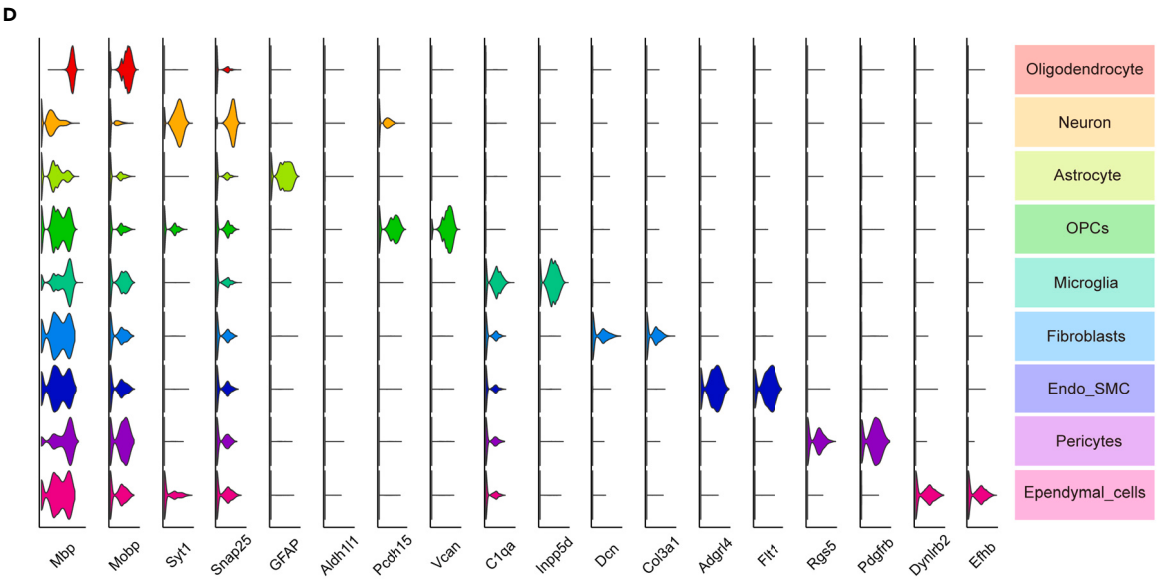
D
Mbp
Mobp
Syt1
Snap25
GFAP
Aldh1l1
Pcdh15
Vcan
C1qa
Inpp5d
Dcn
Col3a1
Adgrl4
Flt1
Rgs5
Pdgfrb
Dynlrb2
Efnb
Oligodendrocyte
Neuron
Astrocyte
OPCs
Microglia
Fibroblasts
Endo_SMC
Pericytes
Ependymal_cells

Figure 1. After SNC in rats, the spinal ventral horn cells on the injured side of the L4-L5 segments exhibited heterogeneity

(A) Schematic diagram of surgical sample scheme and experimental procedure in our study. At different time points after SNC in rats, the left spinal ventral horns of L4-L5 segments were taken out for sequencing and analysis. The groups mentioned later were named as sham, 3 h, 1 day, 3 days, 7 days, and 14 days.

(B) UMAP plot visualizing the cell types and distribution of L4-L5 segments of spinal ventral horn cells of L4-L5 segments after SNC in rats. UMAP plots of different time points showing in Figure S1E.

(C) River diagram showing the dynamic changes in the percentage of 10 different cell types after SNC.

(D) Violin diagram showing the gene markers specifically expressed by different cell types in (B).

JAK-STAT3 pathway.[14] In addition, deletion together with PTEN further promotes axon regeneration.[15] In the adult CNS, many members of the Krüpppel-like transcription factor family (KLFs) affect axon growth. KLF4 is an inhibitor of neurite outgrowth, and hippocampal neurons overexpressing KLF4 exhibited axonal growth retardation, as did KLF9.[16,17] Some members, such as KLF6/7, can promote axonal regeneration.[18] Other transcription factors such as Sox11,[19] Atf3, Gap43,[20] and Jun[21] also play vital roles in axon regeneration.

Recently, single-cell RNA sequencing, as a high-throughput and efficient technical means, can detect the heterogeneity of samples at different developmental and pathological stages at very high resolution, and explore the different transcriptional states of single cells. Several single cell sequencing studies have been performed on injured nerves and DRG after sciatic nerve injury.[22–24] Researchers also have revealed dynamic changes of neural cells in human spinal cord under single cell resolution[25] and cellular heterogeneity of spinal cord after spinal cord injury.[26,27] Significant progress has also been made in single cell spatiotemporal transcriptome analysis. The team of scientists analyzed and compared the process of salamander brain development and regeneration, and constructed the first spatiotemporal map of axolotl brain regeneration.[28]

The heterogeneity in the spinal cord after sciatic nerve crush (SNC) and the cellular response to injury and regeneration in the ventral horn are rarely mentioned. Simultaneously with this study, our team used laser capture microscopy (LCM) combined with Smart-seq2 sequencing (LCM-seq) to construct and reveal the first spatiotemporal profiles of individual motor neurons and their ecological niches *in situ*, providing evidence of axon injury and the dynamic microenvironment information during the regeneration process,[29] but the cells captured by the laser are always not single cells in the full sense, so we then chose the 10X genomics platform. We performed SNC on the left sciatic nerve of the *Sprague-Dawley* (SD) rats, and then took the ventral horn of the spinal L4-L5 segments for single-nuclei RNA sequencing (snRNA-seq). To explore the dynamic changes of gene expression patterns at different stages of SNC, 6 time points were set up (0h, 3h, 1d, 3d, and 7d after SNC respectively, group 0h was defined as sham). We aim to reveal the gene expression changes and molecular expression patterns of the spinal ventral horn motor neurons, as well as other supporting cells involved in regeneration process, then seeking new molecular targets for axon regeneration, which provides a theoretical basis for PNS and CNS regeneration.

RESULTS

Heterogeneity of spinal cord ventral horn cells after SNC

Initially, rats were sacrificed at 0 h, 3 h, 1 day, 3 days, 7 days, and 14 days after SNC to obtain the left spinal ventral horn of the L4-L5 segments (Figure 1A). Our work spanned six time points with three biological replicates at each time point, and 184,772 nuclei were detected in a total of 18 samples after data quality control and efficient filtration (Figure S1A). We performed accurate and unbiased clustering results on the cell populations of the 18 samples, and revealed 30 clusters of cell populations (cluster 0–29) via dimensionality reduction by uniform manifold approximation and projection (UMAP) (Figures S1B and S1C). Totally, 10 cell types, including oligodendrocyte, neurons, astrocyte, OPCs, mircoglia, fibroblasts, endo-SMC, pericytes and ependymal cells were identified in our study based on differentially expressed genes and reported marker genes for specific cells (Figure 1B). The UMAP plots for each of the six time points can be viewed in supplementary materials (Figure S1E). The corresponding cell types of the samples at different time points were completely consistent, but the proportion of different cell types varied slightly. The most dramatic changes in cell numbers occurred in the microglia. Three days after SNC, the number of microglia in the spinal ventral horn increased sharply and remained high until 7 days after SNC, and there was a slight decrease at 14 days (Figure 1C). Neurons in SNC underwent significant gene expression changes, with the largest number of differentially up-regulated genes, and the total number was nearly three times that of other cell types, followed by microglia (Figure S1D). Marker genes specific to each cell type, such as Mobp in oligodendrocyte,[30] Syt1 in neuron,[31] Gfap in astrocyte,[25] Pcdh15 in OPCs, C1qa in microglia,[32]

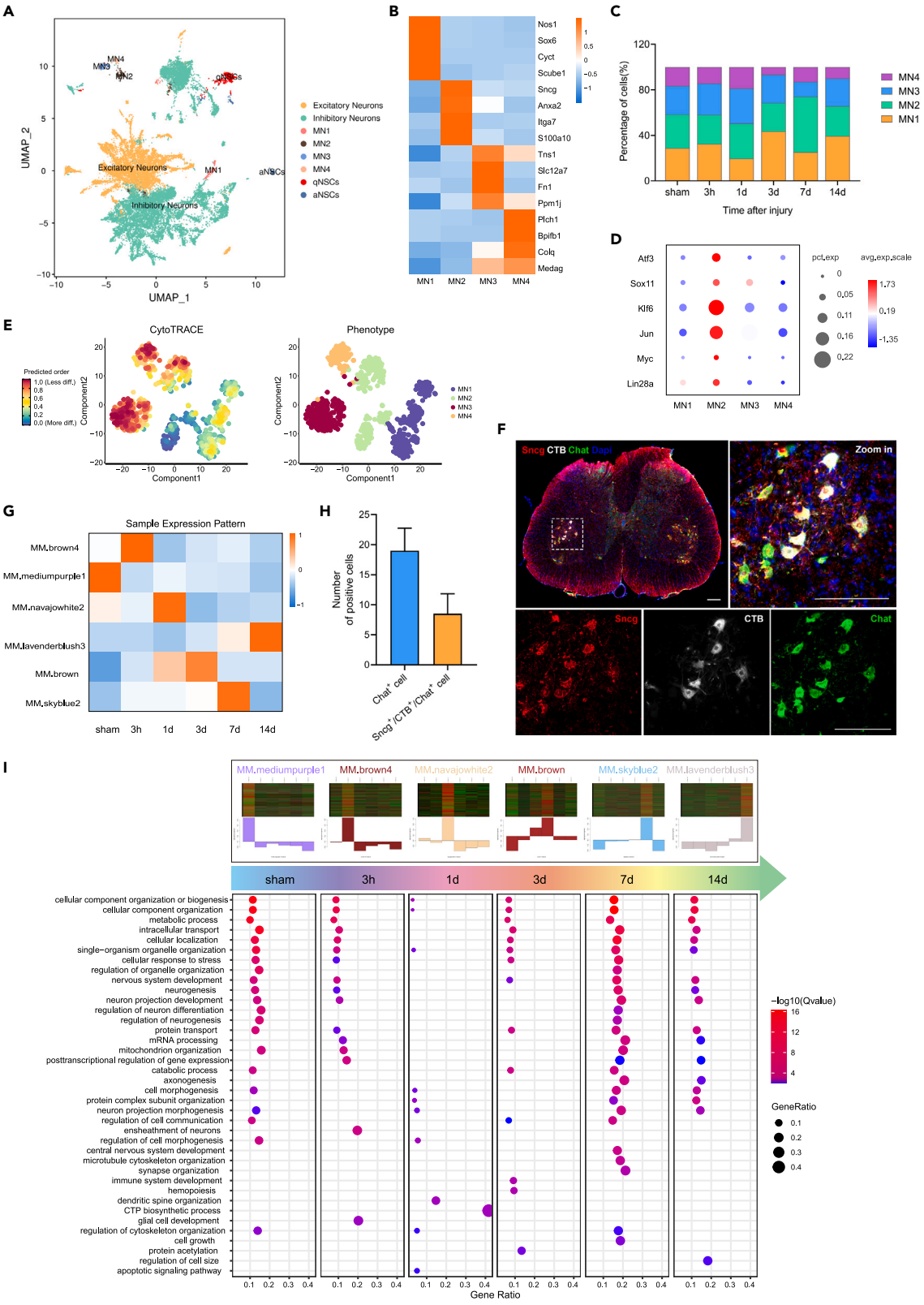
A
UMAP_2
UMAP_1
MN4
MN3
MN2
aNSCs
Excitatory Neurons
MN1
aNSCs
Inhibitory Neurons
Excitatory Neurons
Inhibitory Neurons
MN1
MN2
MN3
MN4
qNSCs
aNSCs
B
Nos1
Sox6
Cyct
Scube1
Sncg
Anxa2
Itga7
S100a10
Tns1
Slc12a7
Fn1
Ppm1j
Plch1
Bpifb1
Colq
Medag
MN1
MN2
MN3
MN4
C
Percentage of cells(%)
Time after injury
sham
3h
1d
3d
7d
14d
MN4
MN3
MN2
MN1
D
Atf3
Sox11
Klf6
Jun
Myc
Lin28a
MN1
MN2
MN3
MN4
pct.exp
avg.exp.scale
E
CytoTRACE
Phenotype
Predicted order
Component1
Component2
MN1
MN2
MN3
MN4
F
Sncg CTB Chat Dapi
Zoom in
Sncg
CTB
Chat
G
Sample Expression Pattern
MM.brown4
MM.mediumpurple1
MM.navajowhite2
MM.lavenderblush3
MM.brown
MM.skyblue2
sham
3h
1d
3d
7d
14d
H
Number of positive cells
Chat+ cell
Sncg+/CTB+/Chat+ cell
I
MM.mediumpurple1
MM.brown4
MM.navajowhite2
MM.brown
MM.skyblue2
MM.lavenderblush3
sham
3h
1d
3d
7d
14d
cellular component organization or biogenesis
cellular component organization
metabolic process
intracellular transport
cellular localization
single-organism organelle organization
cellular response to stress
regulation of organelle organization
nervous system development
neurogenesis
neuron projection development
regulation of neuron differentiation
regulation of neurogenesis
protein transport
mRNA processing
mitochondrion organization
posttranscriptional regulation of gene expression
catabolic process
axonogenesis
cell morphogenesis
protein complex subunit organization
neuron projection morphogenesis
regulation of cell communication
ensheathment of neurons
regulation of cell morphogenesis
central nervous system development
microtubule cytoskeleton organization
synapse organization
immune system development
hemopoiesis
dendritic spine organization
CTP biosynthetic process
glial cell development
regulation of cytoskeleton organization
cell growth
protein acetylation
regulation of cell size
apoptotic signaling pathway
Gene Ratio
−log10(Qvalue)
GeneRatio

Figure 2. After sub-clustering of neurons, MN2 cells were found to be more involved in axon regeneration and various biological processes at different time points after SNC

(A) UMAP plot visualizing the cell types and distribution of neurons. UMAP plots of different time points showing in Figure S2A.
(B) Heatmap showing several top expressed marker genes in 4 motor neuron subtypes.
(C) Bar chart showing the changes in the proportion of cell numbers of various motor neurons at different time points after SNC.
(D) Dotplot showing the expression abundance of several regeneration-associated genes in 4 motor neuron subtypes.
(E) CytoTRACE plot and boxplot showing differentiation potential of four motor neuron suptypes.
(F) Immunofluorescence staining of L4-L5 spinal cord segments after CTB injection. Motor neurons labeled by Chat (green); MN2 labeled by Sncg (red); CTB-positive cells (white); nuclei labeled by Dapi (blue), scale bar = 200 μm.
(G) Heatmap showing gene expression patterns of MN2 at different time points after SNC. The graph was made with the characteristic values of the module. The abscissa was the sample, the ordinate was the module; Orange represented high expression and blue represented low expression.
(H) Bar chart showing number of $Chat^+$ cells and $Sncg^+/CTB^+/Chat^+$ cells after SNC.
(I) Dotplot showing GO enrichment terms of each pattern. The 6 time points corresponded to their respective modules from left to right.

Dcn in fibroblasts,[33] Adgr14 in endo-SMC,[26] Rgs5 in pericytes[27] and Dynlrb2 in ependymal cells[26] were demonstrated in a composite violin diagram. Some rarely reported genes with significantly differentially expressed effects in our study are also shown in our diagram (Figure 1D).

Heterogeneity of neurons in spinal ventral horn and time-dependent gene expression patterns in MN2 after SNC in rats

The sciatic nerve is the extension of the axons of sensory and motor neurons so it is conceivable that once it is damaged, the cell bodies of neurons will react violently. Our team has previously carried out single cell sequencing on sensory neurons after SNC, revealing the molecular regulatory mechanism of axon regeneration in DRG neurons, so this time we concentrated on the changes in gene expression of motor neurons after SNC. We pulled out all of the clusters of neurons that we had previously defined for sub-clustering, and then defined 4 suptypes of motor neuron with different expression patterns (named as MN1-MN4) in the total neuron population (Figures 2A and S2A). By the way, we compared some markers of different types of motor neurons, and then differentially expressed genes from 4 motor neuron suptypes were shown in a heatmap (Figure 2B). In the following paragraphs, we will take these 4 suptypes as the main research objects.

The cell numbers of MN1-MN4 also varied with time after SNC. In general, the number of MN1 cells decreased significantly at 1 day after SNC, but increased again at 3 days. The number of MN2 cells was similar at several other time points, but there was a significant increase at 7 days after SNC. The number of MN3 cells decreased significantly at 7 days, whereas the number of MN4 cells decreased significantly at 3 days (Figure 2C). To investigate whether motor neurons capable of responding and regenerating after SNC concentrated in a specific subtype, we subsequently examined the expression of regeneration-associated genes reported such as Atf3, Sox11, Klf6, Jun, Myc, and Lin28a in our four motor neuron subtypes (Figure 2D). In MN2, these genes showed more significant and higher expression, so we used CytoTRACE (cellular trajectory reconstruction analysis using gene counts and expression) to characterize the differentiation potential of these four subtypes. The results showed that MN2 and MN1 seemed to score higher on the assessment of differentiation potential (Figure 2E). The above suggested to us that MN2 might be a group of motor neurons more involved in axon regeneration in our SNC model.

We injected fluorescein-conjugated CTB (Cholera toxin subunit B) into the distal epineurium of the injured sciatic nerves, so that CTB could be retrograde transported to the cell body of the neuron along the regenerated axons after injury. Immunofluorescence staining of L4-L5 spinal cord segments showed that the number of CTB-positive motor neurons in the ventral horn of the injured side were less than Chat-positive motor neurons, that is to say, after 14 days of SNC, some motor neuron axons still did not break through the crush wound and extended to the proximal portion. Different from MN1, MN3 and MN4, Sncg, and Anxa2 can be used as markers for MN2 cells in MN2. MN2 labeled with Sncg have more co-localization with CTB positive signals, further confirming that the axons of MN2 cells underwent regeneration after SNC (Figures 2F and 2H).

To explore the different expression patterns of motor neuron genes after SNC, genes in MN2 were divided into 7 different modules at 6 time points via weighted gene co-expression network analysis (WGCNA), and at least one module was associated with each time point (Figures 2G and S2B). GO enrichment analysis was performed for genes contained in different modules, and then significantly enriched GO terms were listed. We found that in the sham group main enrichment of the module for the cellular component organization, metabolic, and nervous system development, the organism development and other biological processes

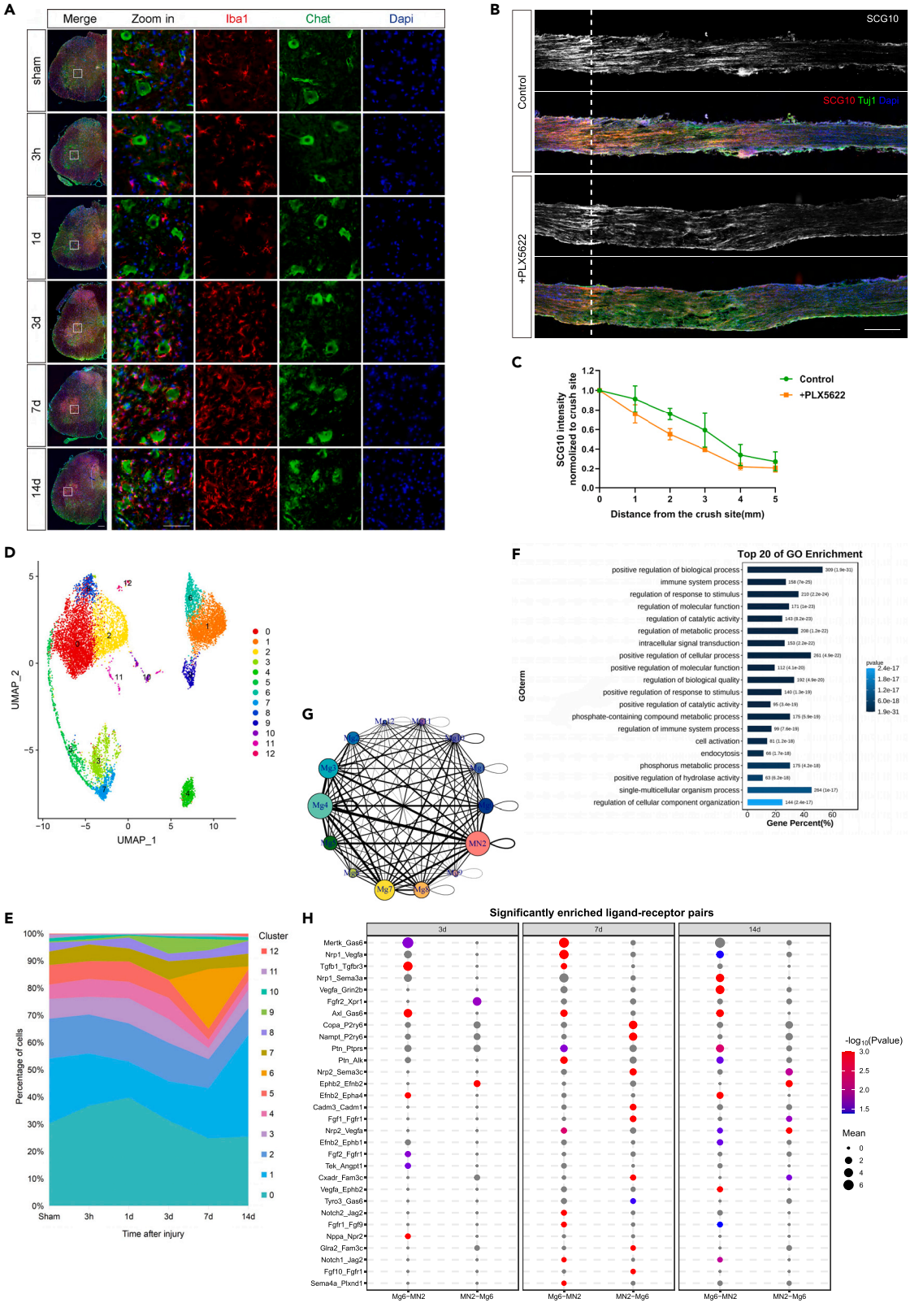
A
Merge
Zoom in
Iba1
Chat
Dapi
sham
3h
1d
3d
7d
14d
B
Control
+PLX5622
SCG10
SCG10 Tuj1 Dapi
C
SCG10 intensity normolized to crush site
Distance from the crush site(mm)
Control
+PLX5622
D
UMAP_2
UMAP_1
E
Percentage of cells
Time after injury
Cluster
F
Top 20 of GO Enrichment
positive regulation of biological process
immune system process
regulation of response to stimulus
regulation of molecular function
regulation of catalytic activity
regulation of metabolic process
intracellular signal transduction
positive regulation of cellular process
positive regulation of molecular function
regulation of biological quality
positive regulation of response to stimulus
positive regulation of catalytic activity
phosphate-containing compound metabolic process
regulation of immune system process
cell activation
endocytosis
phosphorus metabolic process
positive regulation of hydrolase activity
single-multicellular organism process
regulation of cellular component organization
GOterm
Gene Percent(%)
pvalue
G
MN1
MN2
Mg1
Mg2
Mg3
Mg4
Mg5
Mg6
Mg7
Mg8
Mg9
H
Significantly enriched ligand-receptor pairs
3d
7d
14d
Mertk_Gas6
Nrp1_Vegfa
Tgfb1_Tgfbr3
Nrp1_Sema3a
Vegfa_Grin2b
Fgfr2_Xpr1
Axl_Gas6
Copa_P2ry6
Nampt_P2ry6
Ptn_Ptprs
Ptn_Alk
Nrp2_Sema3c
Efnb2_Efnb2
Efnb2_Epha4
Cadm3_Cadm1
Fgf1_Fgfr1
Nrp2_Vegfa
Efnb2_Ephb1
Fgf2_Fgfr1
Tek_Angpt1
Cxadr_Fam3c
Vegfa_Ephb2
Tyro3_Gas6
Notch2_Jag2
Fgfr1_Fgf9
Nppa_Npr2
Glra2_Fam3c
Notch1_Jag2
Fgf10_Fgfr1
Sema4a_Plxnd1
Mg6-MN2
MN2-Mg6
-log10(Pvalue)
Mean

Figure 3. Microglia reacted violently in the spinal ventral horn after SNC and cell communication between MN2 and MG6 occurred

(A) Immunofluorescence staining of microglia in spinal L4-L5 segments. Motor neurons labeled by Chat (green); microglia labeled by Iba1 (red); nuclei labeled by Dapi (blue), scale bar = 200 μm.

(B) Immunofluorescence staining showing sciatic nerve regeneration was inhibited after microglial depletion. Crush site marked by white dashed line; axon labeled by Tuj1 (green); regenerative axon labeled by SCG10 (red); nuclei labeled by Dapi (blue), scale bar = 500 μm.

(C) Line chart showing relative SCG10 intensity at different distances from the crush site (n = 3 independent experiments).

(D) UMAP plot visualizing the cell types and distribution of microglia by time point.

(E) River diagram showing the dynamic changes in the percentage of different clusters of microglia at different time points of SNC.

(F) Bar chart showing the top 20 significantly enriched GO terms of Mg6.

(G) Diagram showing cell interaction network between MN2 and Mg6. Bubbles represented cell types, and the size of bubbles was determined by the number of significantly enriched ligand-receptor pairs between cell types and all their interacting types. Larger bubbles indicated stronger association of cell types in the population. The thickness of the line was determined by the number of significantly enriched ligand-receptor pairs among cell types. Thicker lines represented stronger communication relationship between cell types.

(H) Dotplot showing significantly enriched ligand-receptor pairs between MN2 and Mg6. The size of the dots represented the mean of expression quantity in 2 cell types, and the color of the dots represented the significance of enrichment.

related to the normal survival and activity of motor neurons. Once the sciatic nerve was injured, these biological processes necessary for survival began to slow down, and after 7 days they seemed to slowly return to normal state. As the time point closest to the SNC, the cell response to external stimuli has already appeared 3 h after SNC. The biological processes related to neuronal ensheathment are also active. In the navajowhite2 module, we enriched terms related to CTP biosynthesis, as it has been reported that increased CTP synthase activity could promote neurite growth.[34] Corresponding to the sample of 3 days, we captured the genes of brown module, and enriched more terms related to nervous system development, meanwhile, immune and protein-related processes were vigorous. CNS development, microtubule organization and axongenesis processes were brisk at 7 days. When it came to the 14th day, most enriched GO terms were analogous to the sham group.

Microglia reacted violently in the spinal ventral horn after SNC and many highly abundant ligand-receptor pairs emerged between MN2 and Mg6

Previous results showed that the cell numbers changed significantly after SNC were the microglia (Figure 1C). In the nervous system, microglia exist as immune cells, and presumably react very violently after injury.[35] We also verified the expression of microglia in the ventral horn after SNC. We found that as time went on, the number of microglia gradually increased on the injured side. Starting from the third day, we found that microglia increasingly approached and surrounded motor neurons, and this phenomenon was still observed at 7 days and 14 days (Figure 3A). To more clearly explore the role of microglia in our SNC model, sciatic nerve regeneration was observed 3 days after SNC in mice depleted of microglia by PLX5622, a CSF1R antagonist. It was found that in the absence of microglia (Figures S3A and S3B), the regenerating axons of the injured sciatic nerve were reduced (Figures 3B and 3C). All microglia were then captured a divided into 13 subtypes (Figure 3D), and a new subtype, named Mg6, emerged at 3 days after SNC and reached significant numbers at 7 days (Figure 3E). Top 20 GO enrichment terms showed quite a number of terms related to immune stress (Figures 3F and S3C). Since Mg6 just appeared at 3 days and there were not many cells, we only showed the communication network of MN2 and Mg6 of 7 days (Figures 3G and 3H), and the abundance of significantly enriched ligand-receptor pairs showed after the appearance of Mg6 at 3 days, 7 days, and 14 days. The enrichment of Tgfb1 and its receptor expression in 3 days and 7 days samples suggested that Mg6 may be associated with the axon regeneration of MN2 motor neurons through TGF-β pathway after SNC. Gas6 (growth arrest specific protein 6) is a growth factor widely expressed in the nervous system.[36] Its putative ligands (Axl, Mertk, and Tyro3) were all observed in ligand-receptor pairs that were highly enriched in Mg6 and MN2. Axl-Gas6 pairs were highly expressed at any time after the presence of Mg6. Efnb2 regulated peripheral T cell differentiation, as well as transduction of IL-6 signaling.[37] Given its superior immune activity in other systems,[38] Ephb2-Efnb2, Efnb2-Epha4 expressed in MN2 and Mg6 must also play important roles in inflammation and immunity after SNC. The Notch signaling pathway has been reported to be involved in the communication between glia and neurons.[39] After SNC, the expression of the two ligand-receptor pairs (Notch1-Jag2, Notch2-Jag2) of the Notch pathway was high at 7 days (Figure 3G).

The association of OPCs on the pseudo-time axis with motor neurons, especially MN2, indicated possibility that OPC were involved in axon regeneration after SNC

In earlier years, studies have demonstrated that oligodendrocytes cultured *in vitro* can give rise to neurons and astrocytes, and oligodendrocytes.[40,41] *In vivo*, adult OPCs generate small numbers of neurons throughout the ventral forebrain, especially in the piriform cortex.[42] Cluster2 (C2) was the largest group

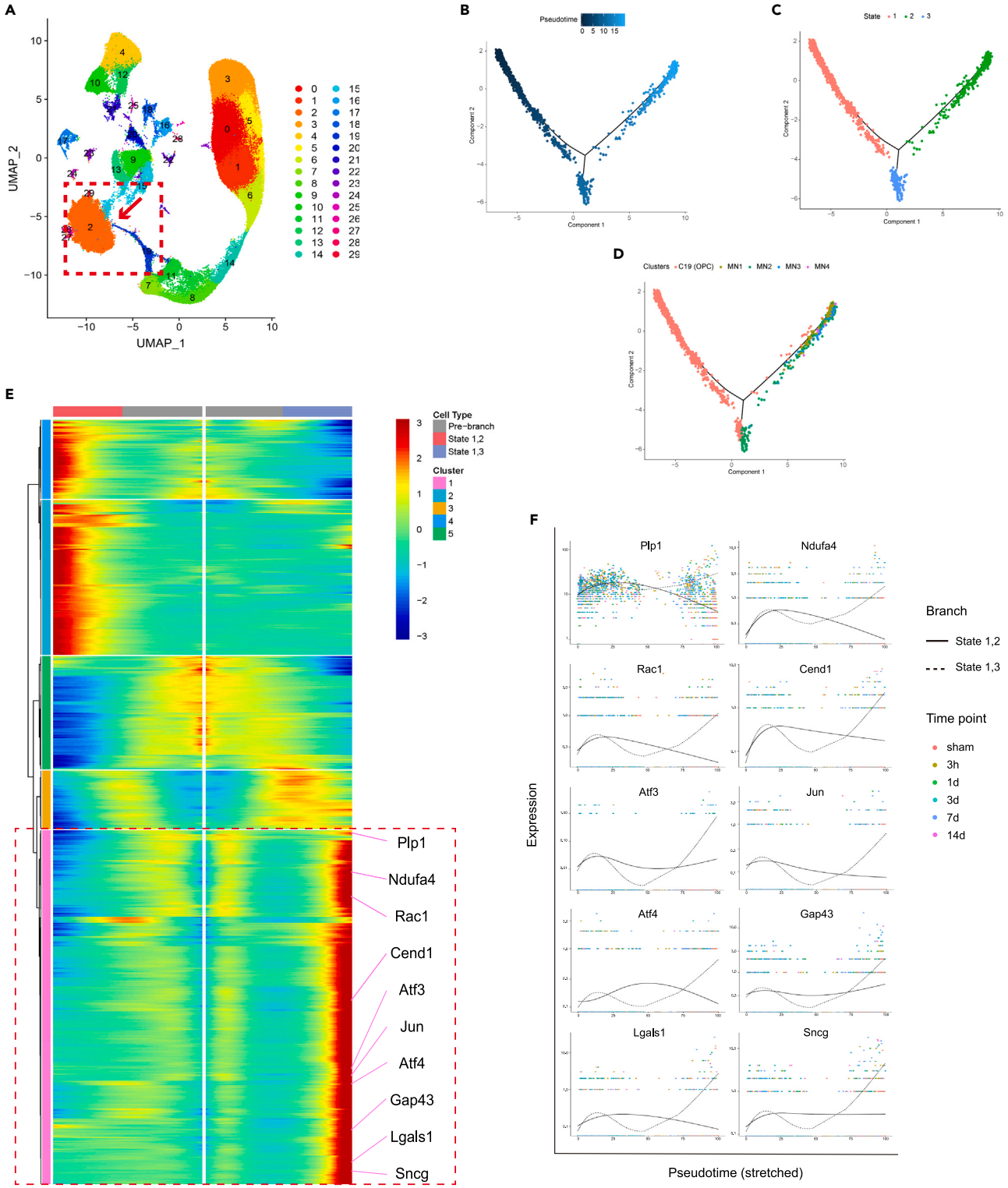

Figure 4. The association of OPCs on the pseudo-time axis with motor neurons, especially MN2, indicated the possibility that OPC were involved in axon regeneration after SNC

(A) UMAP plot showing the connection between C2 (neuron) and C19 (OPCs).

(B) Trajectory plot showing the pseudo-time trend. As the color became lighter, pseudo-time gradually marched.

(C) Trajectory plot showing location and distribution of different cell types.

Figure 4. *Continued*

(D) Trajectory plot showing different states in different cell types.

(E) Heatmap showing different expression patterns based on the branch and several typical genes in cluster 1 were listed.

(F) Scatterplot showing the pseudo-time differences in gene expression, with solid lines representing state1, 2 branching direction and dashed lines representing state1, 3 branching direction.

of neurons in the initial population, and cluster19 (C19) was defined as one of the OPCs subtypes (Figure S1C). We found some cross-linking between C2 and C19 in UMAP, suggesting whether there is a lineage association between neurons and OPCs after SNC in spinal ventral horn (Figure 4A). We combined MN1-4 and C19 cells for pseudo-time analysis (Figure 4B). We found that all cells have only one branchpoint in the trajectory. At this branchpoint, cells went to 2 different fates and were divided into 3 states in the trajectory. C19 cells were mainly distributed in state 1 and state 3, and a small amount in state 2. The 4 MN subtypes have different distributions. MN1, MN3, and MN4 were all distributed in state 2 which was at the later stage of the pseudo-time. Unlike them, a large part of MN2 cells and a part of C19 belonged to state 3 (Figures 4C, 4D, and S4). Gene expression differential analysis was then performed based on the branches, and the gene expression heatmap divided gene expression into 5 different expression patterns. We were more concerned about the gene expression of state 3, of which genes were lowly expressed in pre-branch and state 2 and increased abruptly in state 3, so several genes of the cluster 1 were taken out for further analysis (Figure 4E). Plp1 is highly expressed in state1 and state3, and more abundant in state3. PLP is present in exosomes released by oligodendrocytes and can be taken up by neurons and other glial cells.[43,44] It is possible that elevated OPCs expression of Plp1 enhances communication between oligodendrocytes and neurons through these approaches, thus ensuring the integrity of neurons and OPCs. In CNS, Gal-1(Galectin-1) promotes basal and kainate-induced neural precursor cell proliferation in dentate gyrus of the mouse hippocampus.[45] Rac1 (Rac family small GTPase 1) controls actin dynamics and is closely related to cell proliferation and migration.[46] Krüppel-like factor 2 (Klf2) was induced by Ca^{2+} retrograde signaling in damaged axons, and can promote the transcription of Vav1 by activating Rac1 to promote axon regeneration in dorsal root ganglion (DRG) neurons after SNC.[47] Ndufa4 (NADH dehydrogenase ubiquinone 1 alpha subcomplex 4) inhibited neuronal apoptosis by increasing the expression of Bcl-2 and reducing the expression of cytochrome *c*, and triggered the expression of neurotrophic factors to promote the growth of neurons *in vitro*.[48] Over-expression of Cend1 (cell-cycle exit and neuronal differentiation 1) in neural precursor cells or neuroblastoma cells promotes neuronal differentiation.[49,50] Sncg (synuclein gamma, also known as breast cancer-specific gene 1/BCSG1), a member of the synuclein protein family, was thought to play a role in the pathogenesis of Parkinson's disease.[51] In the previous paragraphs, we used it to label MN2 cells based on its specific expression in MN2 (Figure 2F). In addition to the genes discussed above, some genes related to regeneration in the field of nerve regeneration, such as Jun,[21] Gap43,[52] Atf4[53,54] and Atf3[20] (Figure 4F).

Calcium pathway were involved in axonal regeneration in motor neurons and Cacna2d2 inhibited the axon outgrowth of motor neurons

We screened out the transcription factors with the highest expression in the MN2, sorted them by connectivity and added the previously reported regeneration-associated genes into the IPA software to explore the association between MN2 transcription factors and axon regeneration and predict other key regeneration genes related to them. We found that all of these genes had surprisingly strong associations with the calcium pathway. In the network predicted by IPA software, we focused on Cacna2d2 (Figure 5A), which is reported to be a developmental switch that limits axon growth and promotes CNS regeneration when inhibited by systemic administration.[55] We observed its expression after SNC and found that it was expressed in motor neurons and other neurons in the spinal ventral horn. Unfortunately, we did not see a significant trend of expression at different time points after SNC (Figure 5B). To explore whether it has a function in motor neurons, we used siRNA interference fragments to knock down its expression in cultured motor neurons and found that the axon length increased significantly after Cacna2d2 expression was suppressed both in cell sliders (Figures 5C and 5D) and microfluidic devices (Figures 5E and 5F). Gabapentin preconditioning of motor neuron can inhibit calcium influx caused by lysophosphatidic acids (LPA) (Figures S5A and S5B). Meanwhile, we also administered Gabapentin to interfere the proper function of Cacna2d2 systemically, and after 3 days of SNC, we found that the regenerated axons in the treatment group were more pronounced and significant than those in the control group (Figures 5G and 5H).

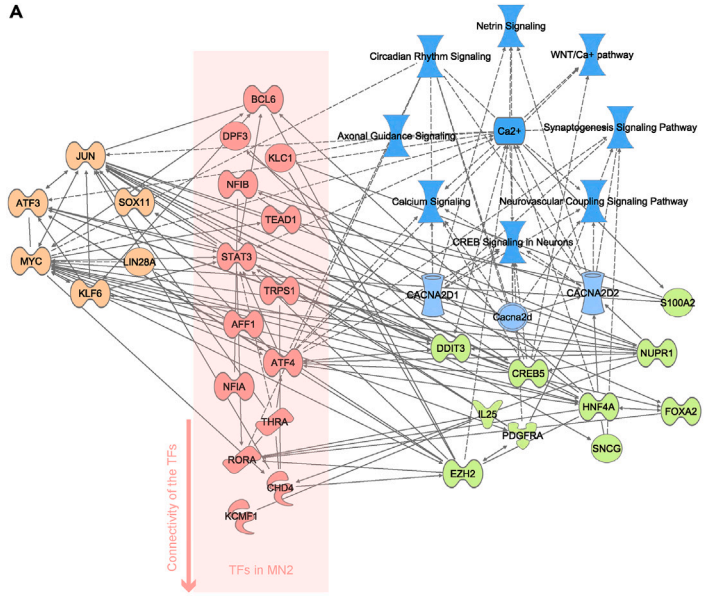
A
Netrin Signaling
Circadian Rhythm Signaling
WNT/Ca+ pathway
Axonal Guidance Signaling
Ca2+
Synaptogenesis Signaling Pathway
Calcium Signaling
Neurovascular Coupling Signaling Pathway
CREB Signaling in Neurons
BCL6
DPF3
KLC1
JUN
NFIB
ATF3
SOX11
TEAD1
MYC
LIN28A
STAT3
KLF6
TRPS1
AFF1
ATF4
NFIA
THRA
RORA
CHD4
KCMF1
EZH2
CACNA2D1
CACNA2D2
Cacna2d
S100A2
DDIT3
NUPR1
CREB5
IL2Ra
HNF4A
FOXA2
PDGFRA
SNCG
Connectivity of the TFs
TFs in MN2

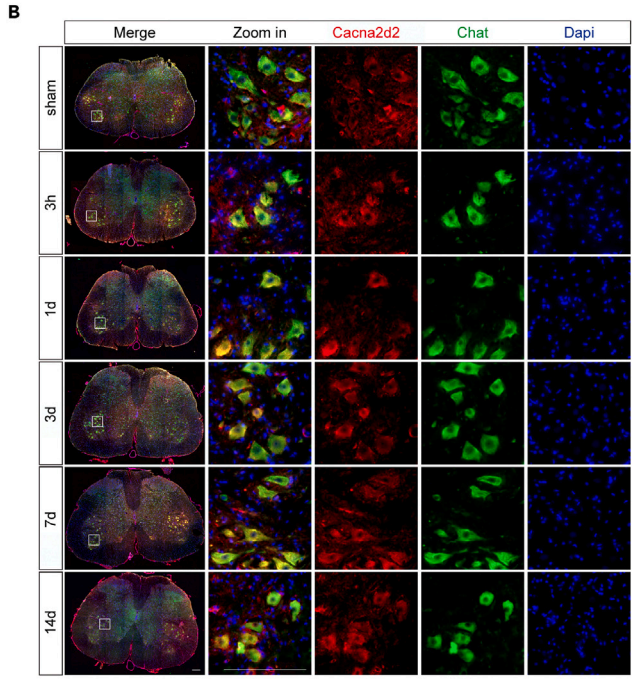
B
Merge
Zoom in
Cacna2d2
Chat
Dapi
sham
3h
1d
3d
7d
14d

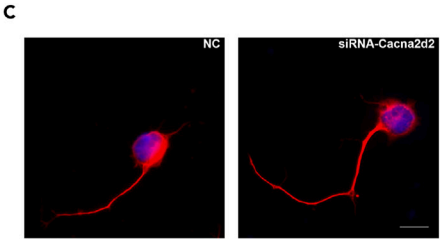
C
NC
siRNA-Cacna2d2

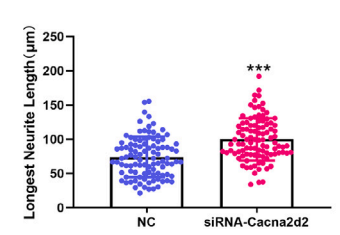
D
Longest Neurite Length (μm)
250
200
150
100
50
0
***
NC
siRNA-Cacna2d2

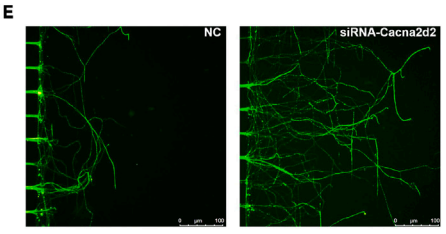
E
NC
siRNA-Cacna2d2

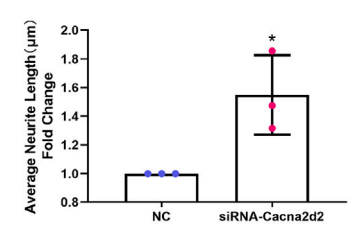
F
Average Neurite Length (μm)
Fold Change
2.0
1.8
1.6
1.4
1.2
1.0
0.8
*
NC
siRNA-Cacna2d2

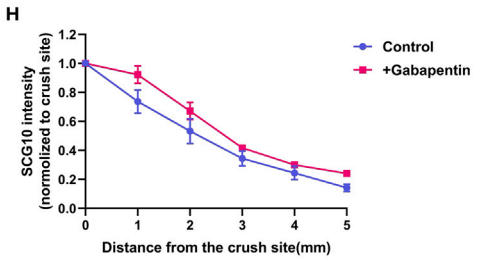
H
SCG10 intensity
(normolized to crush site)
1.2
1.0
0.8
0.6
0.4
0.2
0.0
0
1
2
3
4
5
Distance from the crush site(mm)
Control
+Gabapentin

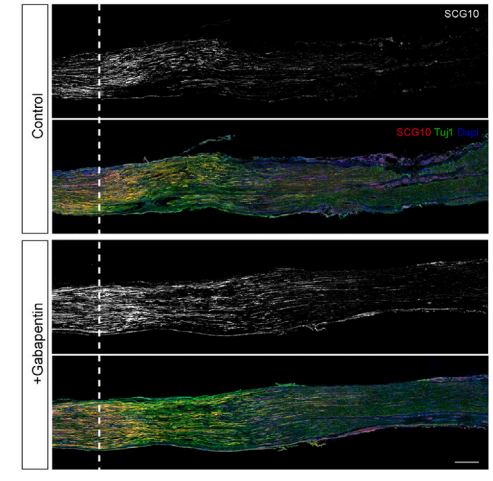
G
Control
+Gabapentin
SCG10
SCG10 Tuj1 Dapi

Figure 5. Calcium pathway were involved in axon regeneration in motor neurons and Cacna2d2 inhibited the axon outgrowth of motor neurons

(A) Network diagram of transcription factors and regeneration-associated genes and pathways in MN2 illustrated the key role of Ca^{2+} pathway.

(B) Immunofluorescence staining showing the location and expression of Cacna2d2. Motor neurons labeled by Chat (green); Cacna2d2 (red); nuclei labeled by Dapi (blue), scale bar = 200 μm.

(C) Immunofluorescence staining showing grow state of cultured motor neurons on cell sliders before and after Cacna2d2 knockdown; scale bar = 10 μm.

(D) Bar chart showing the longest neurite length of single cultured motor neurons in (C); values are mean ± SD (n = 100 independent cells; ***p < 0.001; unpaired t-test).

(E) Immunofluorescence staining showing grow state of cultured motor neurons in microfluidic devices after Cacna2d2 inhibition; axon labeled by Tuj1(green), scale bar = 100 μm.

(F) Bar chart showing average neurite length of single cultured motor neurons in (E); values are mean ± SD (n = 3 independent experiments; *p < 0.05; unpaired t-test).

(G) Immunofluorescence staining showing sciatic nerve regeneration was promoted after intraperitoneal injection of Gabapentin. Crush site marked by white dashed line; axon labeled by Tuj1(green); regenerative axon labeled by SCG10 (red); nuclei labeled by Dapi (blue), scale bar = 500 μm.

(H) Line chart showing relative SCG10 intensity at different distances from the crush site (n = 3 independent experiments).

DISCUSSION

In our study, we used snRNA-seq to comprehensively reveal the heterogeneity of spinal ventral horn cells after SNC. The spinal ventral horn was rich in neuron types and the number of glial cells including microglia, astrocytes, oligodendrocytes, and OPCs varied in post-injury time. Fibroblasts, endo-SMC, pericytes, and ependymal cells were also captured in the results.

Spinal cord integrates the external stimuli received by the sensory nerves, and then the motor nerves transmit motor commands to the target organs. After sciatic nerve injury, sensory neurons and motor neurons respond strongly, and neurons that escape the fate of death still experience profound transcriptional changes accompanied by ultrastructural changes focused on the endoplasmic reticulum and other organelles.[56] The temporal development of sensory neuron-based neuropathic pain has been revealed at the single cell sight.[33] Neurons are the subject of axon regeneration, and we focus more on the gene expression patterns of axon regeneration in motor neurons. We re-clustered the neurons of ventral horn and got 4 motor neuron suptypes. The positive signal of CTB retrograde tracing produced good colocalization with Sncg. Intrinsic capacity of axon regeneration is regulated by transcriptional changes in response to injury,[57] and by comparing the expression of differentially expressed genes (DEGs) that have been widely reported during regeneration. MN2 was found to have more regenerative potential.[19–21,58–61] Having determined the regenerative capacity of MN2, we characterized the biological processes involved in MN2 at different time points after SNC. On the first day after motor neuron axon injury, routine biological activities such as metabolism were partially blocked. This stage is mainly responsible for the biosynthesis of energy required for regeneration and is considered as the preparation period for regeneration. And then the early stages of regeneration continue into the third day for the required ion exchange and protein transport, and of course there are also signs of an immune response. Maintenance of neuronal morphology was initiated upon injury, and axon formation continued at 7 days and 14 days. These evidences revealed the gene expression patterns of motor neurons during different stages after SNC.

After PNI, microglia are activated and recruited to the injury, a phenomenon that correlates positively with the severity of the injury.[62,63] After SNC, the number of microglia increased sharply at 3 days, and there was no sign of decline at 7 days and 14 days. This tight communication has also been addressed in previous studies, including microglia activation next to the DRG.[56,64,65] After microglia depletion, the lag of sciatic nerve regeneration after injury also confirmed the positive role of microglia in axonal regeneration. Calcium influx is a necessary and sufficient condition for inducing axonal degeneration after axonal injury.[66,67] Damaged single neurons trigger calcium elevations in adjacent microglia within a 50 μm radius, mediated by purinergic receptors and intracellular calcium storage.[68] As one of the major purinergic receptors expressed by microglia, after P2ry12 mutation, the response of microglia to focal injury was attenuated, while brain injury-induced changes in somatic connections trigger P2ry12 receptor-dependent microglia glial-neuroprotection, regulating neuronal calcium loading and functional connectivity.[69]

We found that a subset of C19 OPCs and MN2 motor neurons share the same state (state 2) on the trajectory, suggesting that these cells share similar cell fate and gene expression patterns. We discussed some of the genes that are significantly enriched for expression in state 2. During early postnatal development, both $CaV_{1.2}$ and $CaV_{1.3}$ channels are active in OPCs, and these channels mediate multiple aspects of OPC development, such as OPCs survival, proliferation, myelin protein expression levels, and directed migration.[70,71]

The spontaneous and transient elevation of intracellular Ca^{2+} concentration in the early stage is essential in neuronal development and is also critical in neuronal differentiation.[72] Surprisingly, there were several genes closely linked to calcium ions. Cacna2d1 promoted synaptogenesis via postsynaptic Rac1. In the rat dorsal hippocampus, CaMKK1/CaMKIα participated in actin cytoskeleton remodeling and behavioral plasticity by activation of Rac1. The association with calcium in similar DEG in state 2 motor neurons and OPCs after SNC suggested that the control of differentiation of OPCs and the axonal regeneration of motor neurons are both regulated by calcium channels. More boldly, now that it has been observed in the piriform cortex,[42] is it possible that calcium may also mediate the movement of OPCs to neurons. Alternatively, OPCs still differentiate into oligodendrocytes as progenitors, and then participate in motor neuron axon regeneration through the cell behavior of oligodendrocytes. The interesting mechanism behind this is worth exploring further.

The expression of cacna2d2 was increased in corticospinal neurons after complete transection of corticospinal axons in corticospinal neurons and was thought to contribute to maladaptive plasticity and impairment of neuronal function.[73] Overexpression of Cacna2d2 impaired axonal growth in cultured DRG neurons *in vitro*, and Cacna2d2 inhibited axon outgrowth through calcium influx through CaV_2 channels.[55] In our subsequent study of transcription factors in MN2, we found that calcium-related pathways were still in a position that cannot be ignored after the IPA interaction network was built. We verified the expression of Cacna2d2 mentioned in the network in the ventral horn of the spinal cord after SNC and found that it is localized in motor neurons and other neurons. We wondered whether behaviors that direct axonal regeneration by controlling calcium homeostasis are also present in motor neurons after SNC. However, it seemed that the motor neurons in the SNC condition were not fatally damaged, so that the expression of Cacna2d2 in the motor neurons did not change significantly. Nevertheless, we still wanted to explore the effect of Cacna2d2 on axon growth of motor neurons, inhibition of Cacna2d2 expression promoted motor neuron axon growth *in vitro* and interfence of Cacna2d2 function accelerated the growth of sciatic nerve after SNC. This provides guidance for us to use Cacna2d2 as a target to regulate axon regeneration strategies of motor neurons by regulating calcium ion influx in the future.

In summary, our work revealed the heterogeneity of spinal ventral horn cells after SNC, and we identified a regenerated MN2 motor neuron population and gene expression patterns of motor neurons after SNC. Mg6 that react violently and emerge at 3 days after injury have close cell communication with MN2, and OPCs may be involved in axonal regeneration as the supply of motor neurons via calcium pathway (Figure 6). These findings will provide us with more theoretical basis and further research direction for axon regeneration.

Limitations of the study

Although we have proposed three stages of motor neuron axon regeneration after SNC, the molecular mechanism of each stage remains to be further explored in our later work. When revealing the heterogeneity of spinal ventral horn cells, we focused on multiple potential candidate markers (whether in motor neurons or microglia), but we failed to identify specific molecules during experimental verification. We still need further effort to find specific subtype markers through more experimental means to provide meager guidance for the repair and regeneration of PNS and CNS.

STAR★METHODS

Detailed methods are provided in the online version of this paper and include the following:

- KEY RESOURCES TABLE
- RESOURCE AVAILABILITY
  - Lead contact
  - Materials availability
  - Data and code availability
- EXPERIMENTAL MODEL AND STUDY PARTICIPANT DETAILS
  - Animals and surgery
  - Sampling and treatment of tissue
- METHOD DETAILS
  - CTB injection
  - Drug treatments

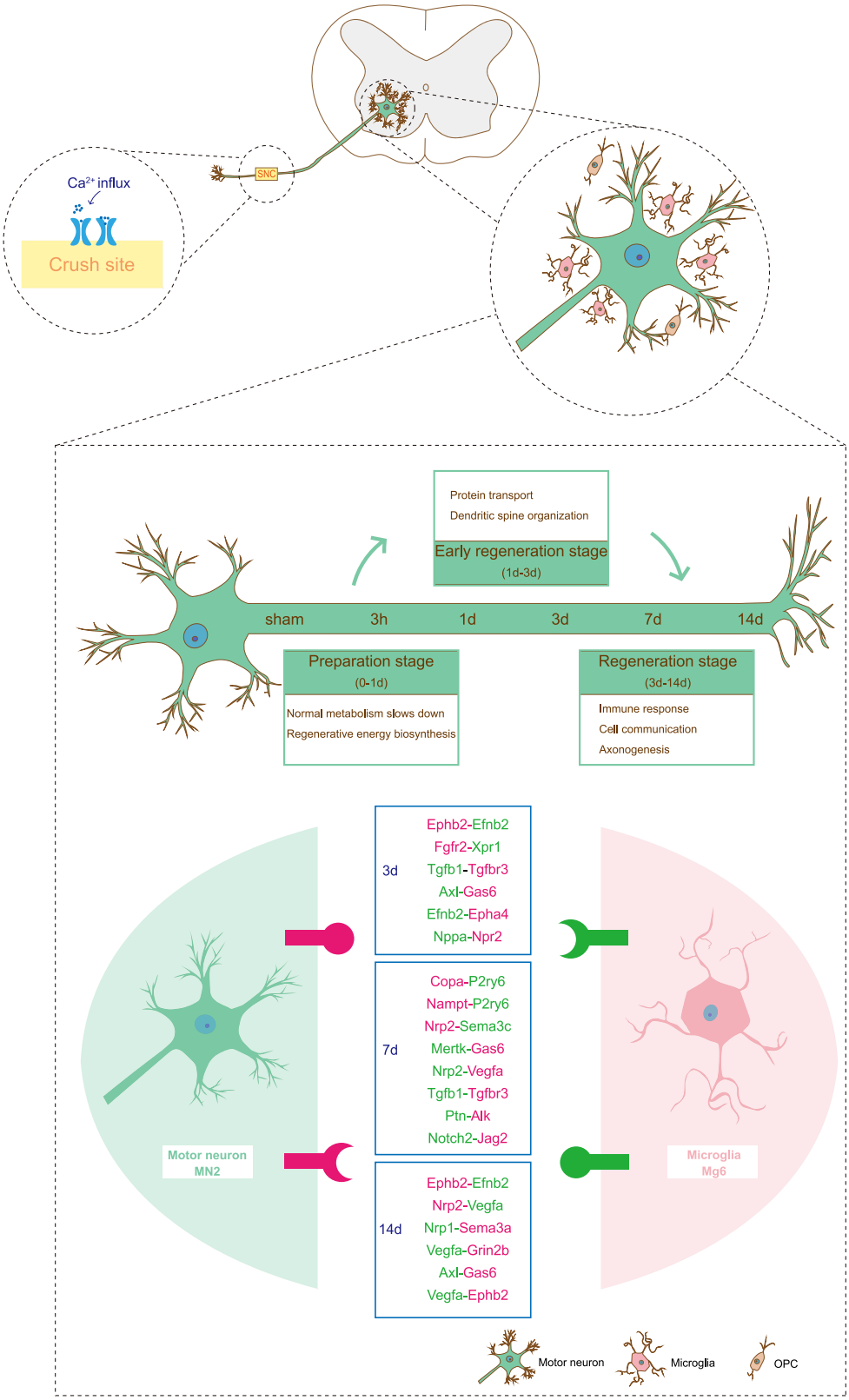

Figure 6. An overview and summary of our study.

- Immunofluorescence staining
- Isolation and culture of primary motor neurons
- Neurite outgrowth of spinal motor neurons *in vitro* in microfluidic device
- siRNA transfection, neurite staining and length statistics of primary spinal motor neurons
- Calcium imaging
- Construction of the single cell standard library
- Analysis of up-regulated genes
- Weighted gene co-expression network analysis (WGCNA)
- Cell communication analysis
- Cell trajectory analysis
- Ingenuity pathway analysis (IPA)

● QUANTIFICATION AND STATISTICAL ANALYSIS

SUPPLEMENTAL INFORMATION

Supplemental information can be found online at https://doi.org/10.1016/j.isci.2023.107264.

ACKNOWLEDGMENTS

This work was supported by the National Natural Science Foundation of China (31730031, 32130060, and 81870975), the National Major Project of Research and Development (2022YFA1105500), and the Natural Science Foundation of Jiangsu Province (BK20202013). We thank GENE DENOVO Company (Guangzhou, Guangdong, China) for bioinformatics analysis support with OmicShare Analysis Platform (http://www.omicshare.com/tools).

AUTHOR CONTRIBUTIONS

Conceptualization, X.G. and S.Z.; Methodology, Y.G., X.G., and S.Z.; Investigation, Y.Z., C.L., L.G., X.W., H.S., Z.C., Q.Z., C.L., Q.S., and S.Z.; Resources, H.S., X.S., and S.Z.; Validation, Y.Z., C.L., L.G., and X.W.; Writing – Original Draft, Y.Z. and C.L.; Writing – Review and Editing, Y.Z., C.L., X.G., and S.Z.; Visualization, Y.Z. and C.L.; Supervision, X.G. and S.Z.; Funding Acquisition, X.G. and S.Z.

DECLARATION OF INTERESTS

The authors declare no competing interests.

Received: November 17, 2022
Revised: May 2, 2023
Accepted: June 27, 2023
Published: July 3, 2023

REFERENCES

1. Hu, P., Bembrick, A.L., Keay, K.A., and McLachlan, E.M. (2007). Immune cell involvement in dorsal root ganglia and spinal cord after chronic constriction or transection of the rat sciatic nerve. Brain Behav. Immun. *21*, 599–616. https://doi.org/10.1016/j.bbi.2006.10.013.

2. Huebner, E.A., and Strittmatter, S.M. (2009). Axon regeneration in the peripheral and central nervous systems. Results Probl. Cell Differ. *48*, 339–351. https://doi.org/10.1007/400_2009_19.

3. Mar, F.M., Bonni, A., and Sousa, M.M. (2014). Cell intrinsic control of axon regeneration. EMBO Rep. *15*, 254–263. https://doi.org/10.1002/embr.201337723.

4. Chen, P., Piao, X., and Bonaldo, P. (2015). Role of macrophages in Wallerian degeneration and axonal regeneration after peripheral nerve injury. Acta Neuropathol. *130*, 605–618. https://doi.org/10.1007/s00401-015-1482-4.

5. Richardson, P.M., and Verge, V.M. (1986). The induction of a regenerative propensity in sensory neurons following peripheral axonal injury. J. Neurocytol. *15*, 585–594. https://doi.org/10.1007/BF01611859.

6. Ylera, B., Ertürk, A., Hellal, F., Nadrigny, F., Hurtado, A., Tahirovic, S., Oudega, M., Kirchhoff, F., and Bradke, F. (2009). Chronically CNS-injured adult sensory neurons gain regenerative competence upon a lesion of their peripheral axon. Curr. Biol. *19*, 930–936. https://doi.org/10.1016/j.cub.2009.04.017.

7. Brosius Lutz, A., and Barres, B.A. (2014). Contrasting the glial response to axon injury in the central and peripheral nervous systems. Dev. Cell *28*, 7–17. https://doi.org/10.1016/j.devcel.2013.12.002.

8. Ghosh-Roy, A., Wu, Z., Goncharov, A., Jin, Y., and Chisholm, A.D. (2010). Calcium and cyclic AMP promote axonal regeneration in Caenorhabditis elegans and require DLK-1 kinase. J. Neurosci. *30*, 3175–3183. https://doi.org/10.1523/JNEUROSCI.5464-09.2010.

9. Kamber, D., Erez, H., and Spira, M.E. (2009). Local calcium-dependent mechanisms determine whether a cut axonal end assembles a retarded endbulb or competent growth cone. Exp. Neurol. *219*, 112–125. https://doi.org/10.1016/j.expneurol.2009.05.004.

10. Neumann, B., Coakley, S., Giordano-Santini, R., Linton, C., Lee, E.S., Nakagawa, A., Xue, D., and Hilliard, M.A. (2015). EFF-1-mediated regenerative axonal fusion requires components of the apoptotic pathway. Nature *517*, 219–222. https://doi.org/10.1038/nature14102.

11. Nawabi, H., Belin, S., Cartoni, R., Williams, P.R., Wang, C., Latremolière, A., Wang, X., Zhu, J., Taub, D.G., Fu, X., et al. (2015). Doublecortin-like kinases promote neuronal survival and induce growth cone reformation via distinct mechanisms. Neuron *88*, 704–719. https://doi.org/10.1016/j.neuron.2015.10.005.

12. Park, K.K., Liu, K., Hu, Y., Smith, P.D., Wang, C., Cai, B., Xu, B., Connolly, L., Kramvis, I., Sahin, M., and He, Z. (2008). Promoting axon regeneration in the adult CNS by modulation of the PTEN/mTOR pathway. Science *322*, 963–966. https://doi.org/10.1126/science.1161566.

13. Christie, K.J., Webber, C.A., Martinez, J.A., Singh, B., and Zochodne, D.W. (2010). PTEN inhibition to facilitate intrinsic regenerative outgrowth of adult peripheral axons. J. Neurosci. *30*, 9306–9315. https://doi.org/10.1523/JNEUROSCI.6271-09.2010.

14. Smith, P.D., Sun, F., Park, K.K., Cai, B., Wang, C., Kuwako, K., Martinez-Carrasco, I., Connolly, L., and He, Z. (2009). SOCS3 deletion promotes optic nerve regeneration in vivo. Neuron *64*, 617–623. https://doi.org/10.1016/j.neuron.2009.11.021.

15. Bei, F., Lee, H.H.C., Liu, X., Gunner, G., Jin, H., Ma, L., Wang, C., Hou, L., Hensch, T.K., Frank, E., et al. (2016). Restoration of visual function by enhancing conduction in regenerated axons. Cell *164*, 219–232. https://doi.org/10.1016/j.cell.2015.11.036.

16. Moore, D.L., Blackmore, M.G., Hu, Y., Kaestner, K.H., Bixby, J.L., Lemmon, V.P., and Goldberg, J.L. (2009). KLF family members regulate intrinsic axon regeneration ability. Science *326*, 298–301. https://doi.org/10.1126/science.1175737.

17. Apara, A., Galvao, J., Wang, Y., Blackmore, M., Trillo, A., Iwao, K., Brown, D.P., Jr., Fernandes, K.A., Huang, A., Nguyen, T., et al. (2017). KLF9 and JNK3 interact to suppress axon regeneration in the adult CNS. J. Neurosci. *37*, 9632–9644. https://doi.org/10.1523/JNEUROSCI.0643-16.2017.

18. Blackmore, M.G., Wang, Z., Lerch, J.K., Motti, D., Zhang, Y.P., Shields, C.B., Lee, J.K., Goldberg, J.L., Lemmon, V.P., and Bixby, J.L. (2012). Kruppel-like Factor 7 engineered for transcriptional activation promotes axon regeneration in the adult corticospinal tract. Proc. Natl. Acad. Sci. USA *109*, 7517–7522. https://doi.org/10.1073/pnas.1120684109.

19. Norsworthy, M.W., Bei, F., Kawaguchi, R., Wang, Q., Tran, N.M., Li, Y., Brommer, B., Zhang, Y., Wang, C., Sanes, J.R., et al. (2017). Sox11 expression promotes regeneration of some retinal ganglion cell types but kills others. Neuron *94*, 1112–1120.e4. https://doi.org/10.1016/j.neuron.2017.05.035.

20. Moore, D.L., and Goldberg, J.L. (2011). Multiple transcription factor families regulate axon growth and regeneration. Dev. Neurobiol. *71*, 1186–1211. https://doi.org/10.1002/dneu.20934.

21. Lerch, J.K., Martínez-Ondaro, Y.R., Bixby, J.L., and Lemmon, V.P. (2014). cJun promotes CNS axon growth. Mol. Cell. Neurosci. *59*, 97–105. https://doi.org/10.1016/j.mcn.2014.02.002.

22. Renthal, W., Tochitsky, I., Yang, L., Cheng, Y.C., Li, E., Kawaguchi, R., Geschwind, D.H., and Woolf, C.J. (2020). Transcriptional reprogramming of distinct peripheral sensory neuron subtypes after axonal injury. Neuron *108*, 128–144.e9. https://doi.org/10.1016/j.neuron.2020.07.026.

23. Wolbert, J., Li, X., Heming, M., Mausberg, A.K., Akkermann, D., Frydrychowicz, C., Fledrich, R., Groeneweg, L., Schulz, C., Stettner, M., et al. (2020). Redefining the heterogeneity of peripheral nerve cells in health and autoimmunity. Proc. Natl. Acad. Sci. USA *117*, 9466–9476. https://doi.org/10.1073/pnas.1912139117.

24. Chen, B., Banton, M.C., Singh, L., Parkinson, D.B., and Dun, X.P. (2021). Single cell transcriptome data analysis defines the heterogeneity of peripheral nerve cells in homeostasis and regeneration. Front. Cell. Neurosci. *15*, 624826. https://doi.org/10.3389/fncel.2021.624826.

25. Zhang, Q., Wu, X., Fan, Y., Jiang, P., Zhao, Y., Yang, Y., Han, S., Xu, B., Chen, B., Han, J., et al. (2021). Single-cell analysis reveals dynamic changes of neural cells in developing human spinal cord. EMBO Rep. *22*, e52728. https://doi.org/10.15252/embr.202152728.

26. Ikeda-Yorifuji, I., Tsujioka, H., Sakata, Y., and Yamashita, T. (2022). Single-nucleus RNA sequencing identified cells with ependymal cell-like features enriched in neonatal mice after spinal cord injury. Neurosci. Res. *181*, 22–38. https://doi.org/10.1016/j.neures.2022.04.006.

27. Milich, L.M., Choi, J.S., Ryan, C., Cerqueira, S.R., Benavides, S., Yahn, S.L., Tsoulfas, P., and Lee, J.K. (2021). Single-cell analysis of the cellular heterogeneity and interactions in the injured mouse spinal cord. J. Exp. Med. *218*, e20210040. https://doi.org/10.1084/jem.20210040.

28. Wei, X., Fu, S., Li, H., Liu, Y., Wang, S., Feng, W., Yang, Y., Liu, X., Zeng, Y.Y., Cheng, M., et al. (2022). Single-cell Stereo-seq reveals induced progenitor cells involved in axolotl brain regeneration. Science *377*, eabp9444. https://doi.org/10.1126/science.abp9444.

29. Zhang, Y., Xu, L., Li, X., Chen, Z., Chen, J., Zhang, T., Gu, X., and Yang, J. (2022). Deciphering the dynamic niches and regeneration-associated transcriptional program of motoneurons following peripheral nerve injury. iScience *25*, 104917. https://doi.org/10.1016/j.isci.2022.104917.

30. Blum, J.A., Klemm, S., Shadrach, J.L., Guttenplan, K.A., Nakayama, L., Kathiria, A., Hoang, P.T., Gautier, O., Kaltschmidt, J.A., Greenleaf, W.J., and Gitler, A.D. (2021). Single-cell transcriptomic analysis of the adult mouse spinal cord reveals molecular diversity of autonomic and skeletal motor neurons. Nat. Neurosci. *24*, 572–583. https://doi.org/10.1038/s41593-020-00795-0.

31. Alkaslasi, M.R., Piccus, Z.E., Hareendran, S., Silberberg, H., Chen, L., Zhang, Y., Petros, T.J., and Le Pichon, C.E. (2021). Single nucleus RNA-sequencing defines unexpected diversity of cholinergic neuron types in the adult mouse spinal cord. Nat. Commun. *12*, 2471. https://doi.org/10.1038/s41467-021-22691-2.

32. Tansley, S., Uttam, S., Ureña Guzmán, A., Yaqubi, M., Pacis, A., Parisien, M., Deamond, H., Wong, C., Rabau, O., Brown, N., et al. (2022). Single-cell RNA sequencing reveals time- and sex-specific responses of mouse spinal cord microglia to peripheral nerve injury and links ApoE to chronic pain. Nat. Commun. *13*, 843. https://doi.org/10.1038/s41467-022-28473-8.

33. Wang, K., Wang, S., Chen, Y., Wu, D., Hu, X., Lu, Y., Wang, L., Bao, L., Li, C., and Zhang, X. (2021). Single-cell transcriptomic analysis of somatosensory neurons uncovers temporal development of neuropathic pain. Cell Res. *31*, 904–918. https://doi.org/10.1038/s41422-021-00479-9.

34. Carter, J.M., Demizieux, L., Campenot, R.B., Vance, D.E., and Vance, J.E. (2008). Phosphatidylcholine biosynthesis via CTP:phosphocholine cytidylyltransferase 2 facilitates neurite outgrowth and branching. J. Biol. Chem. *283*, 202–212. https://doi.org/10.1074/jbc.M706531200.

35. Prinz, M., Jung, S., and Priller, J. (2019). Microglia biology: one century of evolving concepts. Cell *179*, 292–311. https://doi.org/10.1016/j.cell.2019.08.053.

36. Stitt, T.N., Conn, G., Gore, M., Lai, C., Bruno, J., Radziejewski, C., Mattsson, K., Fisher, J., Gies, D.R., Jones, P.F., et al. (1995). The anticoagulation factor protein S and its relative, Gas6, are ligands for the Tyro 3/Axl family of receptor tyrosine kinases. Cell *80*, 661–670. https://doi.org/10.1016/0092-8674(95)90520-0.

37. Luo, H., Charpentier, T., Wang, X., Qi, S., Han, B., Wu, T., Terra, R., Lamarre, A., and Wu, J. (2011). Efnb1 and Efnb2 proteins regulate thymocyte development, peripheral T cell differentiation, and antiviral immune responses and are essential for interleukin-6 (IL-6) signaling. J. Biol. Chem. *286*, 41135–41152. https://doi.org/10.1074/jbc.M111.302596.

38. Huang, X., Zhang, G., Tang, T., and Liang, T. (2021). Identification of tumor antigens and immune subtypes of pancreatic adenocarcinoma for mRNA vaccine development. Mol. Cancer *20*, 44. https://doi.org/10.1186/s12943-021-01310-0.

39. Sanna, M.D., Borgonetti, V., and Galeotti, N. (2020). mu opioid receptor-triggered Notch-1 activation contributes to morphine tolerance: role of neuron-glia communication. Mol. Neurobiol. *57*, 331–345. https://doi.org/10.1007/s12035-019-01706-6.

40. Raff, M.C., Miller, R.H., and Noble, M. (1983). A glial progenitor cell that develops in vitro into an astrocyte or an oligodendrocyte depending on culture medium. Nature *303*, 390–396. https://doi.org/10.1038/303390a0.

41. Kondo, T., and Raff, M. (2000). Oligodendrocyte precursor cells reprogrammed to become multipotential CNS stem cells. Science *289*, 1754–1757. https://doi.org/10.1126/science.289.5485.1754.

42. Rivers, L.E., Young, K.M., Rizzi, M., Jamen, F., Psachoulia, K., Wade, A., Kessaris, N., and Richardson, W.D. (2008). PDGFRA/NG2 glia generate myelinating oligodendrocytes and piriform projection neurons in adult mice. Nat. Neurosci. *11*, 1392–1401. https://doi.org/10.1038/nn.2220.

43. Harlow, D.E., Saul, K.E., Culp, C.M., Vesely, E.M., and Macklin, W.B. (2014). Expression of proteolipid protein gene in spinal cord stem cells and early oligodendrocyte progenitor cells is dispensable for normal cell migration and myelination. J. Neurosci. *34*, 1333–1343. https://doi.org/10.1523/JNEUROSCI.2477-13.2014.

44. Frühbeis, C., Fröhlich, D., Kuo, W.P., Amphornrat, J., Thilemann, S., Saab, A.S., Kirchhoff, F., Möbius, W., Goebbels, S., Nave, K.A., et al. (2013). Neurotransmitter-triggered transfer of exosomes mediates oligodendrocyte-neuron communication. PLoS Biol. *11*, e1001604. https://doi.org/10.1371/journal.pbio.1001604.

45. Kajitani, K., Nomaru, H., Ifuku, M., Yutsudo, N., Dan, Y., Miura, T., Tsuchimoto, D., Sakumi, K., Kadoya, T., Horie, H., et al. (2009). Galectin-1 promotes basal and kainate-induced proliferation of neural progenitors in the dentate gyrus of adult mouse hippocampus. Cell Death Differ. *16*, 417–427. https://doi.org/10.1038/cdd.2008.162.

46. Ridley, A.J. (2006). Rho GTPases and actin dynamics in membrane protrusions and vesicle trafficking. Trends Cell Biol. *16*, 522–529. https://doi.org/10.1016/j.tcb.2006.08.006.

47. Wang, Q., Gong, L., Mao, S., Yao, C., Liu, M., Wang, Y., Yang, J., Yu, B., Chen, G., and Gu, X. (2021). Klf2-Vav1-Rac1 axis promotes axon regeneration after peripheral nerve injury. Exp. Neurol. *343*, 113788. https://doi.org/10.1016/j.expneurol.2021.113788.

48. Balsa, E., Marco, R., Perales-Clemente, E., Szklarczyk, R., Calvo, E., Landázuri, M.O., and Enríquez, J.A. (2012). NDUFA4 is a subunit of complex IV of the mammalian electron transport chain. Cell Metab. *16*, 378–386. https://doi.org/10.1016/j.cmet.2012.07.015.

49. Politis, P.K., Makri, G., Thomaidou, D., Geissen, M., Rohrer, H., and Matsas, R. (2007). BM88/CEND1 coordinates cell cycle exit and differentiation of neuronal precursors. Proc. Natl. Acad. Sci. USA *104*, 17861–17866. https://doi.org/10.1073/pnas.0610973104.

50. Makri, G., Lavdas, A.A., Katsimpardi, L., Charneau, P., Thomaidou, D., and Matsas, R. (2010). Transplantation of embryonic neural stem/precursor cells overexpressing BM88/Cend1 enhances the generation of neuronal cells in the injured mouse cortex. Stem Cell. *28*, 127–139. https://doi.org/10.1002/stem.258.

51. Clayton, D.F., and George, J.M. (1999). Synucleins in synaptic plasticity and neurodegenerative disorders. J. Neurosci. Res. *58*, 120–129. https://doi.org/10.1002/(sici)1097-4547.

52. Xiong, X.X., Pan, F., Chen, R.Q., Hu, D.X., Qiu, X.Y., Li, C.Y., Xie, X.Q., Tian, B., and Chen, X.Q. (2018). Neuroglobin boosts axon regeneration during ischemic reperfusion via p38 binding and activation depending on oxygen signal. Cell Death Dis. *9*, 163. https://doi.org/10.1038/s41419-017-0260-8.

53. Pasini, S., Corona, C., Liu, J., Greene, L.A., and Shelanski, M.L. (2015). Specific downregulation of hippocampal ATF4 reveals a necessary role in synaptic plasticity and memory. Cell Rep. *11*, 183–191. https://doi.org/10.1016/j.celrep.2015.03.025.

54. Xie, M.X., Cao, X.Y., Zeng, W.A., Lai, R.C., Guo, L., Wang, J.C., Xiao, Y.B., Zhang, X., Chen, D., Liu, X.G., and Zhang, X.L. (2021). ATF4 selectively regulates heat nociception and contributes to kinesin-mediated TRPM3 trafficking. Nat. Commun. *12*, 1401. https://doi.org/10.1038/s41467-021-21731-1.

55. Tedeschi, A., Dupraz, S., Laskowski, C.J., Xue, J., Ulas, T., Beyer, M., Schultze, J.L., and Bradke, F. (2016). The calcium channel subunit Alpha2delta2 suppresses axon regeneration in the adult CNS. Neuron *92*, 419–434. https://doi.org/10.1016/j.neuron.2016.09.026.

56. Salvany, S., Casanovas, A., Piedrafita, L., Tarabal, O., Hernández, S., Calderó, J., and Esquerda, J.E. (2021). Microglial recruitment and mechanisms involved in the disruption of afferent synaptic terminals on spinal cord motor neurons after acute peripheral nerve injury. Glia *69*, 1216–1240. https://doi.org/10.1002/glia.23959.

57. Lee, J., and Cho, Y. (2021). Potential roles of stem cell marker genes in axon regeneration. Exp. Mol. Med. *53*, 1–7. https://doi.org/10.1038/s12276-020-00553-z.

58. Venkatesh, I., Mehra, V., Wang, Z., Simpson, M.T., Eastwood, E., Chakraborty, A., Beine, Z., Gross, D., Cabahug, M., Olson, G., and Blackmore, M.G. (2021). Co-occupancy identifies transcription factor co-operation for axon growth. Nat. Commun. *12*, 2555. https://doi.org/10.1038/s41467-021-22828-3.

59. Shin, H.Y., Kwon, M.J., Lee, E.M., Kim, K., Oh, Y.J., Kim, H.S., Hwang, D.H., and Kim, B.G. (2021). Role of Myc proto-oncogene as a transcriptional Hub to regulate the expression of regeneration-associated genes following preconditioning peripheral nerve injury. J. Neurosci. *41*, 446–460. https://doi.org/10.1523/JNEUROSCI.1745-20.2020.

60. Nathan, F.M., Ohtake, Y., Wang, S., Jiang, X., Sami, A., Guo, H., Zhou, F.Q., and Li, S. (2020). Upregulating Lin28a promotes axon regeneration in adult mice with optic nerve and spinal cord injury. Mol. Ther. *28*, 1902–1917. https://doi.org/10.1016/j.ymthe.2020.04.010.

61. Gong, L., Gu, Y., Han, X., Luan, C., Liu, C., Wang, X., Sun, Y., Zheng, M., Fang, M., Yang, S., et al. (2023). Spatiotemporal dynamics of the molecular expression pattern and intercellular interactions in the glial scar response to spinal cord injury. Neurosci. Bull. *39*, 213–244. https://doi.org/10.1007/s12264-022-00897-8.

62. Nishihara, T., Tanaka, J., Sekiya, K., Nishikawa, Y., Abe, N., Hamada, T., Kitamura, S., Ikemune, K., Ochi, S., Choudhury, M.E., et al. (2020). Chronic constriction injury of the sciatic nerve in rats causes different activation modes of microglia between the anterior and posterior horns of the spinal cord. Neurochem. Int. *134*, 104672. https://doi.org/10.1016/j.neuint.2020.104672.

63. Rotterman, T.M., Akhter, E.T., Lane, A.R., MacPherson, K.P., García, V.V., Tansey, M.G., and Alvarez, F.J. (2019). Spinal motor circuit synaptic plasticity after peripheral nerve injury depends on microglia activation and a CCR2 mechanism. J. Neurosci. *39*, 3412–3433. https://doi.org/10.1523/JNEUROSCI.2945-17.2019.

64. De Luca, C., Savarese, L., Colangelo, A.M., Bianco, M.R., Cirillo, G., Alberghina, L., and Papa, M. (2016). Astrocytes and microglia-mediated immune response in maladaptive plasticity is differently modulated by NGF in the ventral horn of the spinal cord following peripheral nerve injury. Cell. Mol. Neurobiol. *36*, 37–46. https://doi.org/10.1007/s10571-015-0218-2.

65. Kalinski, A.L., Yoon, C., Huffman, L.D., Duncker, P.C., Kohen, R., Passino, R., Hafner, H., Johnson, C., Kawaguchi, R., Carbajal, K.S., et al. (2020). Analysis of the immune response to sciatic nerve injury identifies efferocytosis as a key mechanism of nerve debridement. Elife *9*, e60223. https://doi.org/10.7554/eLife.60223.

66. Scheib, J., and Höke, A. (2013). Advances in peripheral nerve regeneration. Nat. Rev. Neurol. *9*, 668–676. https://doi.org/10.1038/nrneurol.2013.227.

67. George, E.B., Glass, J.D., and Griffin, J.W. (1995). Axotomy-induced axonal degeneration is mediated by calcium influx through ion-specific channels. J. Neurosci. *15*, 6445–6452. https://doi.org/10.1523/jneurosci.15-10-06445.1995.

68. Umpierre, A.D., and Wu, L.J. (2021). How microglia sense and regulate neuronal activity. Glia *69*, 1637–1653. https://doi.org/10.1002/glia.23961.

69. Cserép, C., Pósfai, B., Lénárt, N., Fekete, R., László, Z.I., Lele, Z., Orsolits, B., Molnár, G., Heindl, S., Schwarcz, A.D., et al. (2020). Microglia monitor and protect neuronal function through specialized somatic purinergic junctions. Science *367*, 528–537. https://doi.org/10.1126/science.aax6752.

70. Paez, P.M., and Lyons, D.A. (2020). Calcium signaling in the oligodendrocyte lineage: regulators and consequences. Annu. Rev. Neurosci. *43*, 163–186. https://doi.org/10.1146/annurev-neuro-100719-093305.

71. Cheli, V.T., Santiago González, D.A., Namgyal Lama, T., Spreuer, V., Handley, V., Murphy, G.G., and Paez, P.M. (2016). Conditional deletion of the L-type calcium channel Cav1.2 in oligodendrocyte progenitor cells affects postnatal myelination in mice. J. Neurosci. *36*, 10853–10869. https://doi.org/10.1523/JNEUROSCI.1770-16.2016.

72. Yu, Y.L., Chou, R.H., Chen, L.T., Shyu, W.C., Hsieh, S.C., Wu, C.S., Zeng, H.J., Yeh, S.P., Yang, D.M., Hung, S.C., and Hung, M.C. (2011). EZH2 regulates neuronal differentiation of mesenchymal stem cells through PIP5K1C-dependent calcium signaling. J. Biol. Chem. *286*, 9657–9667. https://doi.org/10.1074/jbc.M110.185124.

73. Sun, W., Larson, M.J., Kiyoshi, C.M., Annett, A.J., Stalker, W.A., Peng, J., and Tedeschi, A. (2020). Gabapentinoid treatment promotes corticospinal plasticity and regeneration following murine spinal cord injury. J. Clin. Invest. *130*, 345–358. https://doi.org/10.1172/JCI130391.

74. Langfelder, P., and Horvath, S. (2008). WGCNA: an R package for weighted correlation network analysis. BMC Bioinformatics *9*, 559. https://doi.org/10.1186/1471-2105-9-559.

75. Qiu, X., Mao, Q., Tang, Y., Wang, L., Chawla, R., Pliner, H.A., and Trapnell, C. (2017). Reversed graph embedding resolves complex single-cell trajectories. Nat. Methods *14*, 979–982. https://doi.org/10.1038/nmeth.4402.

STAR★METHODS

KEY RESOURCES TABLE

REAGENT or RESOURCE	SOURCE	IDENTIFIER
Antibodies		
ChAT Polyclonal Antibody	Invitrogen	Cat# PA5-29653; RRID: AB_2547128
Cacna2d2 Polyclonal Antibody	Invitrogen	Cat# PA5-95536; RRID: AB_2807338
Anti-Mouse Iba1 antibody [EPR16589]	Abcam	Cat# ab283319
Anti-Rabbit Iba1 antibody [EPR16589]	Abcam	Cat# ab178847
Anti-beta III Tubulin antibody [2G10]	Abcam	Cat# ab78078
Stathmin-2/STMN2 (SCG10) Antibody	NOVUS	Cat# NBP1-49461
Cy3-Goat Anti-Rabbit IgG (H + L)	Proteintech	Cat# SA00009-2
Goat anti-Mouse IgG (H + L), Alexa Fluor 488	Invitrogen	Cat #A-11001; RRID: AB_2534069
Donkey Anti-Rabbit IgG, Alexa Fluor 647	Abcam	Cat# ab150075
Dapi-Fluoromount-G	SouthernBiotech	Cat# 0100-20
Biological samples		
Rat spinal cord tissue	Experimental Animal Center of Nantong University, Jiangsu, China	N/A
Chemicals, peptides, and recombinant proteins		
PLX5622	MCE	Cat# HY-114153
Gabapentin	MCE	Cat# HY-A0057
Leibovitz's L-15 Medium	Gibco	Cat# 11415064
Hibernate™®-E Medium	Gibco	Cat# A1247601
Trypsin-EDTA	Gibco	Cat# 25200072
Neurobasal™ Medium	Gibco	Cat# 21103049
Poly-L-lysine Solution Bioreagent	Sigma-Aldrich	Cat# P4832
LPA	Sigma-Aldrich	Cat# L7260
RNAi transfection reagent	Invitrogen	Cat# 13778150
opti-MEM	Invitrogen	Cat# 31985070
CTB	Invitrogen	Cat# C34776
Bovine Serum Albumin	Biofroxx	Cat# 143183
Deposited data		
Raw and processed snRNA-seq data	This paper	GSA: CRA008582
Oligonucleotides		
siRNA targeting sequence: Cacna2d2: CTGACGCTGCAGAGAATTT	Ribobio	N/A
Primer for Cacna2d2: Forward: AGGACCAACCTCAGAAGTGC; Reverse: ATGGGAGGGTGAGCGAAAAG	Sangon Biotech	N/A
Software and algorithms		
Cell Ranger	10X Genomics	Version 3.1.0
Seurat	https://satijalab.org/seurat/	version 3.1.1
CellPhoneDB	https://www.cellphonedb.org	Version 2.0

RESOURCE AVAILABILITY

Lead contact

Further information and requests for resources should be directed to and will be fulfilled by the lead contact, Songlin Zhou (songlin.zhou@ntu.edu.cn).

Materials availability

This study did not generate new unique reagents.

Data and code availability

SnRNA-seq data of this study have been deposited at GSA and are publicly available as of the date of publication. Accession numbers are listed in the key resources table.

This paper does not report original code.

Any additional information required to reanalyze the data reported in this paper is available from the lead contact upon request.

EXPERIMENTAL MODEL AND STUDY PARTICIPANT DETAILS

Animals and surgery

Male SD rats and C57BL/6 mice, 8 weeks of age, were performed SNC on the left sciatic nerves. Rats anesthesia was performed by isoflurane. Then the skin was disinfected and prepared, the skin was cut through the middle thigh of the left hindlimb, the muscle and fascia were bluntly separated, and the sciatic nerve was exposed. The 3 mm crush wound was chiseled perpendicular to the sciatic nerve using a smooth clipping forceps (lasted for 30 s, with an interval of 5 s every 10 s). Mice were anesthetized by special anesthetic (Nanjing AIBI Bio-Technology Co., Ltd, Cat# M2910) for mice and their length of crush wound were set to 2 mm. Spinal cords of L4-L5 segments, where sciatic nerves were emitted, were taken out at 0 h, 3 h, 1 day, 3 days, 7 days and 14 days after SNC. The removed tissue was placed in pre-cooled artificial cerebrospinal fluid, then the vertebrae were peeled under a stereological microscope, and the ventral horn portion of the spinal cord injury side was separated and quickly preserved in liquid nitrogen for subsequent experiments.

Animals were supplied from Experimental Animal Center of Nantong University and were carried out in accordance with Institutional Animal Care Guidelines of Nantong University. The collection of animal tissues shall be ethically approved by the Administration Committee of Experimental Animals (S20200601-903).

Sampling and treatment of tissue

After anesthesia, animals were systemically perfused with normal saline and 4% paraformaldehyde successively via ascending aorta. Spinal cord tissues from L4-L5 segments of animals were placed in 4% paraformaldehyde at 4°C and fixed for 8–12 h. The spinal cord was dehydrated with sucrose solution, frozen with embedding agent and cut into 12 μm coronal sections.

METHOD DETAILS

CTB injection

Fourteen days after SNC, the rats were anesthetized and the fascia and muscle were carefully separated to expose the sciatic nerve after a 1.5cm skin incision on the posterior side of the left femur. Then, 2 μL of 1% CTB (Invitrogen, Cat# C3477) was slowly injected into the distal epineurium of the crush wound, and the whole injection process lasted about 20 s. After remaining in place for 3–4 min, the tip was pulled out slowly to prevent the tracer from being exposed. The rats were then sacrificed 3 days after injection to collected tissues.

Drug treatments

Mice were intraperitoneally injected with PLX5622 (MCE, Cat# HY-114153) at a dose of 50 mg/kg for 14 days, and the subsequent SNC was constructed. The mice were continuously administered until they were sacrificed. Control mice were intraperitoneally injected daily with a mixture of blank solvents from the reagent company's official solution protocol.

Rats were intraperitoneally injected with gabapentin (MCE, Cat# HY-A0057) at a dose of 50 mg/kg immediately after SNC and then daily until sacrifice. Control rats were intraperitoneally injected with the same volume of PBS.

Immunofluorescence staining

After the sections were thoroughly washed in PBS, they were blocked with blocking solution (5% BSA, 10% donkey serum, 0.1% Triton X-100) for 90 min at room temperature. The primary antibodies were then incubated overnight at 4°C, washed 3 times with PBS, and then incubated with the corresponding secondary antibodies for 90 min at room temperature. After washing off excess secondary antibody with PBS, the slides were mounted with Dapi-Fluoromount-G (SouthernBiotech, Cat# 0100-20) to simultaneously label the nuclei.

Isolation and culture of primary motor neurons

Spinal motor neurons were obtained from rat embryos at 13.5 days of gestation. The embryos were removed from the uterus and immediately placed in pre-cooled L15 medium. The spinal cords were carefully removed under anatomical microscope, dissected and meninges were carefully teared, and then fully sheathed and digested with 0.25% trypsin at 37°C for 30 min. Filtered with a 70 μm aperture, gently added the filtered liquid in equal volume to the upper layer of motor neuron separation solution (15% NycoPreP$^{1.077}$ + 83% HE medium +2% B27) (non-mixing), centrifuged at 2000 RPM for 15 min, then washed the precipitation. Relatively pure motor neurons can be obtained.

Neurite outgrowth of spinal motor neurons *in vitro* in microfluidic device

The sterile microfluidic devices were adhered to the PLL precoated Petri dish in advance, and 5μL suspension of spinal motor neurons (cell density of 3×10^5/mL) was added to the upper left and lower right wells of the microfluidic device, respectively. After 4 h culture in the incubator, siRNA fragment was added, and fluid was changed at an interval of 16 h. After the axon completely grew to the right axon chamber for 4 days, the vacuum rod was used to suction the axon chamber three times, each time lasting 1–2 min, during which bubbles were avoided, and the suction vacuum pressure was >18 inch-Hg to ensure that the axon was completely crosscut. Then the cells were cultured for 24 h and fixed for subsequent axon staining and statistics.

siRNA transfection, neurite staining and length statistics of primary spinal motor neurons

The corresponding siRNA fragments (Ribobio), RNAi transfection reagent (Invitrogen, Cat# 13778150) and opti-MEM (Invitrogen, Cat# 13778150) were gently mixed and evenly in accordance with the proportion recommended by the instructions 15 min in advance, and the fusion was placed at room temperature. The mixture was then added to the cell culture plate, and the primary cell suspension was added. After 14 h culture in the incubator, the transfection system was removed and replaced with conventional neuron culture medium for about 20 h. After the cells were cleaned with PBS, they were fixed with 4% PFA at room temperature for 30 min. After washing with PBS for 2 times, immunofluorescence blocker was used for sealing for 90 min. Then Tuj1 primary antibody was added and incubated for 16 h at 4°C. After cleaning with PBS, corresponding fluorescent secondary antibody was replaced, incubated at room temperature for 1 h. Residual antibody was washed by PBS and sealed with anti-fluorescence quenching sealing solution, and images were taken under fluorescence microscope. For axon length statistics, ImageJ software was used to set different data points for recording and statistics according to experimental requirements.

Calcium imaging

Gabapentin (100 μM) pretreated primary motor neurons for 36h, and calcium ion indicator (Abcam, Cat# ab112129) would show the changes of Ca^{2+} in neurons after axon injury caused by LPA (Sigma-Aldrich, Cat# L7260) in the form of fluorescence. After the addition of LPA (2 μM), fluorescence imaging of living cells was performed immediately, generating an image every 30s for 100 cycles under a confocal microscope (Zeiss, LSM900).

Construction of the single cell standard library

After adjusting the number of cells to no less than 1000/μL using an automated counter, load the cell suspension on a 10X Genome Chromium single-cell instrument, add barcoded gel beads and mix reagents, and mix components in a microfluidic "double cross" system. The crossover system is coated with oil-surfactant

droplets to form GEMs, which flow into the reservoir to be collected, and the gel beads dissolve to release sequences for subsequent reverse transcription. Following the traditional next-generation sequencing process, sequencing joint P5 and sequencing primer R1 were added to the cDNA product, and a standard library was constructed after PCR amplification and the constructed library was subjected to high-throughput sequencing operation using the paired-end sequencing mode of the Illumina sequencing platform. High-quality cells were filtered, canonical correspondence analysis (CCA) and *Z* score normalization were used to correct the batch effect, integrate and normalize data. Principal component analysis (PCA) was used to reduce variables and dimensionality. For intuitive analysis of the data, the cells were clustered and grouped and visualized by UMAP.

Analysis of up-regulated genes

Seurat's Bimod likelihood ratio statistical test was used to analyze the differential expression of genes in different cell types, and to screen the up-regulated genes. Screening conditions: the gene was expressed in more than 25% of the target cell types; p value ≤ 0.01; gene expression fold change $\log_2 FC \geq 0.360674$.

Weighted gene co-expression network analysis (WGCNA)

WGCNA was performed using the WGCNA (v1.47) R package.[74] Calculate the correlation coefficient with the sample or sample traits through the module eigengenes, and find the significant modules. The intra-module connectivity (K.in) and module association (MM) of each gene were calculated and correlation analysis was performed using the module characteristic genes and specific trait or phenotype data. For the most relevant modules corresponding to each phenotype data, the Pearson correlation between each gene and the trait data under the module is calculated, and the gene significance value is obtained. Then we performed GO enrichment analysis on the genes in each module, and then made bubble plots selectively for biological process GO terms.

Cell communication analysis

Cell communication analysis was performed using cellphone DB to analyze the expression abundance of ligand-receptor interactions between two cell types based on receptor expression in one cell type and ligand expression in another cell type. A cellular interaction network map was constructed by capturing the number and expression of significantly enriched ligand-receptor pairs between cell types.

Cell trajectory analysis

Single cell trajectory analysis was performed using matrix of cells and gene expressions by monocle (Version2.10.1, http://cole-trapnell-lab.github.io/monocle-release/). The gene expression matrix generated by 10x Genomics was imported into monocle, and the parameters were adjusted to reduce the dimension, and the cell differentiation trajectory was constructed. The cell trajectories were visualized for different differentiation states, different samples and different cell subsets, and presented as a tree-like structure containing tips and branches.[75]

Further gene expression differential analysis was performed on the branches (FDR<1^{e-7}), key genes were screened, and then the branch-dependent genes were subjected to hierarchical clustering analysis to show the change trend of gene expression with the branch. Clade differential genes were selected according to their significance, and the trajectories of the expression levels of the branch differential genes with the pseudo-time line were displayed.

Ingenuity pathway analysis (IPA)

We used IPA China software for gene network construction, and the software automatically assigned default molecular logo shapes to genes in the constructed network, and we autonomously assigned different colors to genes with different functions, so as to finally present the network diagram.

QUANTIFICATION AND STATISTICAL ANALYSIS

Bioinformatic analysis was described in the method details section. Statistical data analysis was performed by Student's *t* test using GraphPad Prism (Version 8.0.2), and more samples and analysis information can be found in the corresponding figure legends.